

1 **Real-time measurements of gas-phase organic acids using SF₆⁻ chemical ionization**
2 **mass spectrometry**

3
4 Theodora Nah,^{1,a} Yi Ji,^{1,2} David J. Tanner,¹ Hongyu Guo,¹ Amy P. Sullivan,³ Nga Lee
5 Ng,^{1,2} Rodney J. Weber¹ and L. Gregory Huey^{1*}

6
7 ¹*School of Earth and Atmospheric Sciences, Georgia Institute of Technology, Atlanta, GA, USA*

8 ²*School of Chemical and Biomolecular Engineering, Georgia Institute of Technology, Atlanta, GA, USA*

9 ³*Department of Atmospheric Science, Colorado State University, Fort Collins, CO, USA*

10 ^a*Now at School of Energy and Environment, City University of Hong Kong, Kowloon, Hong Kong, China*

11 ** To whom correspondence should be addressed: greg.huey@eas.gatech.edu*

12
13 **Abstract**

14 The sources and atmospheric chemistry of gas-phase organic acids are currently poorly
15 understood due in part to the limited range of measurement techniques available. In this
16 work, we evaluated the use of SF₆⁻ as a sensitive and selective chemical ionization reagent
17 ion for real-time measurements of gas-phase organic acids. Field measurements are made
18 using a chemical ionization mass spectrometer (CIMS) at a rural site in Yorkville, Georgia
19 from September to October 2016 to investigate the capability of this measurement
20 technique. Our measurements demonstrate that SF₆⁻ can be used to measure a range of
21 organic acids in the atmosphere. 1-hour averaged ambient concentrations of organic acids
22 ranged from a few parts per trillion by volume (ppt) to several parts per billion by volume
23 (ppb). All the organic acids displayed similar strong diurnal behaviors, reaching maximum
24 concentrations between 5 and 7 pm local time. The organic acid concentrations are
25 dependent on ambient temperature, with higher organic acid concentrations being
26 measured during warmer periods.

27 **Introduction**

28 Organic acids are ubiquitous and important species in the troposphere. They are
29 major contributors of free acidity in precipitation (Galloway et al., 1982; Keene et al., 1983;
30 Keene and Galloway, 1984), and can also affect the formation of secondary organic
31 aerosols (SOA) (Zhang et al., 2004; Carlton et al., 2006; Sorooshian et al., 2010; Yatavelli
32 et al., 2015). As end products of oxidation, organic acids can also serve as useful tracers of
33 air mass history (Sorooshian et al., 2007; Sorooshian et al., 2010). Organic acids are found
34 in urban, rural and remote marine environments in the gas, aqueous and particle phases.

35 While organic acids are emitted directly from biogenic sources (e.g., microbial activity,
36 vegetation and soil) and anthropogenic activities (e.g., fossil fuel combustion, vehicular
37 emissions and biomass burning) (Kawamura et al., 1985; Talbot et al., 1988; Chebbi and
38 Carlier, 1996; Talbot et al., 1999; Seco et al., 2007; Veres et al., 2010; Paulot et al., 2011;
39 Veres et al., 2011; Millet et al., 2015), they can also be formed from photooxidation of
40 non-methane volatile organic compounds and aqueous-phase photochemistry of semi-
41 volatile organic compounds (Chebbi and Carlier, 1996; Hansen et al., 2003; Orzechowska
42 and Paulson, 2005; Carlton et al., 2006; Sorooshian et al., 2007; Ervens et al., 2008; Paulot
43 et al., 2011; Millet et al., 2015). The chemical aging of organic aerosols has also been
44 proposed as a major source of organic acids (Molina et al., 2004; Vlasenko et al., 2008;
45 Paulot et al., 2011). The relative importance of primary and secondary sources of organic
46 acids are currently poorly constrained though their emissions likely depend on the
47 magnitude of biogenic and anthropogenic activities and the meteorological conditions. Wet
48 and dry deposition are the primary sinks of organic acids in the atmosphere (Chebbi and
49 Carlier, 1996).

50 Formic and acetic acids are the dominant gas-phase monocarboxylic acids in the
51 troposphere (Chebbi and Carlier, 1996). Due to their high vapor pressures, the gas-phase
52 concentrations of formic and acetic acids are usually 1 to 2 orders of magnitudes higher
53 than their particle-phase concentrations. Some field studies report strong correlations
54 between formic and acetic acids, suggesting that these two organic acids have similar
55 sources (Nolte et al., 1997; Souza and Carvalho, 2001; Paulot et al., 2011). A recent
56 modeling study suggested that the dominant sources of formic acid in the southeastern U.S.
57 are primarily biogenic in nature (Millet et al., 2015). These sources include direct emissions
58 from vegetation and soil and photochemical production from biogenic volatile organic
59 compounds (BVOCs). Currently, atmospheric formic and acetic acid concentrations are
60 higher than those predicted by models, indicating that present model estimates of source
61 and sink magnitudes are incorrect (Paulot et al., 2011; Millet et al., 2015). In the case of
62 formic acid, deposition and secondary photochemical production via mechanisms such as
63 photooxidation of isoprene and reaction of stabilized criegee intermediates need to be
64 better constrained in models. Given that formic and acetic acids are major trace gases in
65 the atmosphere, there is a need to resolve the discrepancy between measurements and

66 model predictions to close the atmospheric reactive carbon budget and improve our overall
67 understanding of VOC chemistry in the atmosphere.

68 Currently, research on gas-phase organic acids has focused primarily on formic and
69 acetic acids (Andreae et al., 1988; Talbot et al., 1988; Grosjean, 1991; Hartmann et al.,
70 1991; Talbot et al., 1995; Talbot et al., 1999). This is due, in part, to the analytical
71 difficulties in measuring gas-phase $> C_2$ organic acids and oxidized organic acids (i.e.,
72 containing more than 2 oxygen atoms) in real time. These organic acids have low vapor
73 pressures and are generally present in low concentrations in the gas phase. For example,
74 dicarboxylic acids typically have vapor pressures that are 2 to 4 orders of magnitude lower
75 than their analogous monocarboxylic acids (Chebbi and Carlier, 1996), and are present
76 mainly in the particle and aqueous phases. Rapid and accurate measurements of gas-phase
77 $> C_2$ organic acids and oxidized organic acids are necessary for constraining the regional
78 and global SOA budget since these acids can partition readily between the gas and particle
79 and aqueous phases and subsequently affect SOA formation (Zhang et al., 2004; Carlton
80 et al., 2006; Ervens et al., 2008; Sorooshian et al., 2010; Yatavelli et al., 2015).

81 Chemical ionization mass spectrometry (CIMS) is commonly used to selectively
82 measure atmospheric trace gases in real-time with high sensitivity. CIMS measurements
83 rely on reactions between reagent ions and compounds of interest present in the sampled
84 air to produce analyte ions that are detected by a mass spectrometer. The subset of
85 molecular species detected is determined by the reagent ion employed since the specificity
86 of the ionization process is governed by the ion-molecule reaction mechanism. CIMS is a
87 popular tool for atmospheric measurements since it is versatile and has high time resolution
88 and sensitivity. It is also often a soft ionization technique with minimal ion fragmentation,
89 thus preserving the parent molecule's elemental composition and allowing for molecular
90 speciation. Recent developments in chemical ionization methods and sources have greatly
91 improved our ability to measure atmospheric acidic species. Some of the CIMS reagent
92 ions that have been used to measure atmospheric organic acids include acetate ($CH_3CO_2^-$),
93 iodide (I^-) and CF_3O^- anions (Crouse et al., 2006; Veres et al., 2008; Lee et al., 2014;
94 Brophy and Farmer, 2015; Nguyen et al., 2015). However, each of these CIMS reagent
95 ions has its drawbacks, which are generally related to their selectivity and sensitivity

96 towards different atmospheric species. For example, acetic acid is difficult to measure with
97 CH_3CO_2^- as the CIMS reagent ion due to interferences from the reagent ion chemistry that
98 complicates the desired ion-molecule reactions. In addition, while many organic acids can
99 be detected using I^- as a reagent ion, its sensitivity to different acids can vary by orders of
100 magnitude (Lee et al., 2014).

101 The sulfur hexafluoride (SF_6^-) anion has been used as a CIMS reagent ion to
102 measure atmospheric inorganic species such as sulfur dioxide (SO_2), nitric acid (HNO_3)
103 and peroxyxynitric acid (HO_2NO_2) (Slusher et al., 2001; Slusher et al., 2002; Huey et al.,
104 2004; Kim et al., 2007). SF_6^- commonly reacts with most acidic gases at the collision rate
105 by either proton or fluoride transfer reactions (Huey et al., 1995). The SF_6^- ion chemistry
106 is selective to acidic species, which can simplify the mass spectral analysis of organic acids.
107 However, SF_6^- is reactive to both ozone (O_3) and water vapor, which can lead to interfering
108 reactions that limit its applicability to many species in certain environments (Huey et al.,
109 2004). For these reasons, this work is focused on assessing the ability of SF_6^- to measure a
110 series of organic acids in ambient air. The major advantage that SF_6^- has over I^- and
111 CH_3CO_2^- in this study is that it offers the possibility of sensitive detection of acetic and
112 oxalic acids and SO_2 (Lee et al., 2014; Lee et al., 2018). CF_3O^- has a similar chemistry to
113 SF_6^- but it also has issues due to hydrolysis and the ion precursor is not commercially
114 available. We present ambient measurements of gas-phase organic acids conducted in a
115 mixed forest-agricultural area in Georgia in early fall of 2016 to evaluate the performance
116 of a SF_6^- CIMS technique. Gas-phase organic acid measurements are compared to gas-
117 phase water-soluble organic carbon (WSOC_g) measurements performed during the field
118 study to estimate the fraction of WSOC_g that is comprised of organic acids at this rural site.
119 Laboratory experiments are conducted to measure the sensitivity of SF_6^- with a series of
120 organic acids of atmospheric relevance.

121 **2. Methods**

122 **2.1. Field site**

123 Real-time ambient measurements of gas-phase organic acids were obtained using a
124 chemical ionization mass spectrometer from 3 Sept to 12 Oct 2016 at the SouthEastern

125 Aerosol Research and Characterization (SEARCH) site located in Yorkville, Georgia. A
126 detailed description of the field site has been provided by Hansen et al. (2003). Briefly, the
127 Yorkville field site (33.931 N, 85.046 W) was located ~55 km northwest of Atlanta (the
128 closest urban center), and was on a broad ridge in a large pasture where there were
129 occasionally grazing cattle. The field site was surrounded by forest and agricultural land.
130 There were no major roads near the field site and nearby traffic emissions were negligible.
131 The closest power plant was Plant Bowen, which was located ~25 km north of the field
132 site. The sampling period was characterized by moderate temperatures (24.0 °C average,
133 32.6 °C max, 9.5 °C min) and high relative humidities (68.9 % RH average, 100 % RH
134 max, 21.6 % RH min). The study-averaged diurnal trends of relative humidity, temperature
135 and solar radiance are shown in Fig. S1. Data reported are displayed in EDT. Volumetric
136 gas concentrations reported are at ambient temperature and relative humidity.

137 **2.2. SF₆- CIMS**

138 **2.2.1. CIMS instrument and air sampling inlet**

139 The CIMS instrument was housed in a temperature-controlled trailer during the
140 field study. The inlet configuration and CIMS instrument used in this study is shown in
141 Fig. 1. Since HNO₃ and organic acids may condense on surfaces, an inlet configuration
142 with a minimal wall interaction was used. This inlet configuration was previously described
143 by Huey et al. (2004) and Nowak et al. (2006); hence, only a brief description will be
144 provided here. The inlet was a 7.6 cm ID aluminum pipe that extended ~40 cm into the
145 ambient air through a hole in the trailer's wall. This positioned the inlet ~2 m above the
146 ground. A donut-shaped ring was attached to the ambient sampling port of the pipe to
147 reduce the influence of crosswinds on the pipe's flow dynamics. This ring was wrapped
148 with a fine wire mesh to prevent insects from being drawn through the pipe. A flow of
149 ~2800 L min⁻¹ was maintained in the pipe using a regenerative blower (AMETEK
150 Windjammer 116637-03). Part of this flow (7 L min⁻¹) was sampled through a custom-
151 made three-way PFA Teflon valve, which connected the pipe's center to the CIMS
152 sampling orifice. The valve was maintained at a temperature of 40 °C in an insulated
153 aluminum oven and could be switched automatically between ambient and background

154 modes. In ambient mode, ambient air was passed through a 25 cm long, 0.65 cm ID Teflon
155 tube into the CIMS. In background mode, ambient air was first drawn through an activated
156 charcoal scrubber before being delivered into the CIMS. A small flow of ambient air (~ 0.05
157 L min^{-1}) was continuously passed through the scrubber to keep it at equilibrium with
158 ambient humidity levels. Most of the sampled air flow (6.7 L min^{-1}) was exhausted using
159 a small diaphragm pump. The rest of the sampled air flow (0.3 L min^{-1}) was introduced
160 into the CIMS instrument through an automatic variable orifice, which was used to
161 maintain a constant sample air mass flow.

162 The CIMS instrument was comprised of a series of differentially pumped regions:
163 a flow tube, a collisional dissociation chamber, an octopole ion guide, a quadrupole mass
164 filter and an ion detector. These sections were evacuated by a scroll pump (Edward nXDS
165 20i), a drag pump (Adixen MDP 5011) and two turbo pumps (Varian Turbo-V301),
166 respectively. Ambient air was drawn continuously into the flow tube. A flow of 3.7
167 standard liter per minute (slpm) of N_2 containing a few ppm of SF_6 (Scott-Marrin Inc.) was
168 passed through a ^{210}Po ion source into the flow tube. SF_6^- anions, which were produced via
169 associative electron attachment in the ^{210}Po ion source, reacted with the sampled ambient
170 air in the flow tube to generate analyte ions. Arnold and Viggiano (2001) showed that the
171 formation of $\text{F}^{\bullet}(\text{HF})_n$ cluster ions from the reaction of SF_6^- and water vapor is enhanced at
172 high flow tube pressures. Since these $\text{F}^{\bullet}(\text{HF})_n$ cluster ions could interfere with mass
173 spectral analysis, the flow tube was maintained at a low pressure ($\sim 13 \text{ mbar}$, 0.5 %
174 uncertainty) in this study to reduce both the water vapor concentration and reaction time in
175 the flow tube, thus minimizing interferences from SF_6^- reaction with water vapor. The
176 analyte ions exited the flow tube and were accelerated through the collisional dissociation
177 chamber (CDC), which was maintained at $\sim 0.8 \text{ mbar}$ (10 % uncertainty). The molecular
178 collisions in the CDC served to dissociate weakly bound cluster ions into their core ions to
179 simplify mass spectral analysis. Flow tube and CDC pressures were controlled by the
180 automatic variable orifice. For this study, the CDC was operated at a relatively high electric
181 field ($\sim 113 \text{ V cm}^{-1}$) to efficiently dissociate cluster ions. The resulting ions were then
182 passed into the octopole ion guide (maintained at $\sim 6 \times 10^{-3} \text{ mbar}$), which collimated the
183 ions and transferred them into the quadrupole mass spectrometer (maintained at $\sim 10^{-5}$
184 mbar) for mass selection and detection. It should also be noted that we always used gloves

185 when working on the CIMS during this study to limit contamination of lactic acid
186 emissions from human skin. In addition, we kept people away from the front of the SF₆⁻
187 CIMS sampling inlet to minimize lactic acid interferences as well.

188 Ions monitored during the field study included mass-to-charge ratio (m/z) 45, 59,
189 65, 73, 75, 79, 82, 87, 89, 101, 102, 103, 108, 117, 131 and 148. The assignment of these
190 ions will be discussed in section 3. The dwell time for each m/z ion was set to 0.5 s and
191 measurements of these ions were obtained every ~13 s, which resulted in a ~4 % (= 0.5/13
192 x 100 %) duty cycle for each ion monitored. The data presented in this paper was averaged
193 to 1-hour intervals unless stated otherwise.

194 **2.2.2. Background and calibration measurements during field study**

195 Background measurements were performed every 25 min during the field study.
196 During each background measurement, the sampled air flow was passed through an
197 activated charcoal scrubber prior to delivery into the CIMS. The scrubber removed > 99 %
198 of the targeted species in ambient air. Calibration measurements were performed every 5 h
199 during the field study through standard additions of ³⁴SO₂ and either formic or acetic acid
200 to the sampled air flow. Each background and calibration measurement period lasted ~4
201 and ~3.5 min, respectively, which not only gave the scrubber (during background
202 measurements) and flow tube ample time to equilibrate when the three-way PFA Teflon
203 valve was switched between ambient and background modes, but also allowed us to obtain
204 good averaging statistics during background and calibration measurements. A 1.12 ppm
205 ³⁴SO₂ gas standard was used as the source of the sulfur standard addition. 1.85 ppb of ³⁴SO₂
206 was added to sampled air flow during calibration measurements. The formic and acetic
207 acid calibration sources were permeation tubes (VICI Metronics) with emission rates of 91
208 and 110 ng min⁻¹, respectively. The emission rates were measured by scrubbing the output
209 of the permeation tube in deionized water via a gas impinger immersed in water, which
210 was then analyzed for formate and acetate using ion chromatography (Thermo Fisher
211 Scientific). Eight samples of each acid were analyzed over the course of the field study and
212 the standard deviations of the permeation rates were ≤ 6 %. 6.75 ppb of formic acid and
213 5.87 ppb of acetic acid was added to sampled air flow during calibration measurements.
214 The CIMS instrument sensitivity measured by the F₂³⁴SO₂⁻ ion signal (m/z 104) was

215 similarly applied to all the other measured species (except for formic and acetic acids)
216 using relative sensitivities determined in laboratory studies. The $F_2^{34}SO_2^-$ calibrant ion
217 signals were also used to calibrate ambient $F_2^{32}SO_2^-$ ion signals and determine ambient SO_2
218 concentrations as discussed in section 3.2.5.

219 **2.2.3. Laboratory calibration**

220 To estimate the levels of sensitivities for a series of acids of atmospheric relevance,
221 HNO_3 , oxalic, butyric, glycolic, propionic and valeric acid standard addition calibrations
222 were performed in post-field laboratory work. Many of these acids have previously been
223 measured in rural and urban environments (Kawamura et al., 1985; Veres et al., 2011;
224 Brophy and Farmer, 2015). The response of the CIMS acid signals were measured relative
225 to the sensitivity of $^{34}SO_2$ in these calibration measurements. The HNO_3 calibration source
226 was a permeation tube (KIN-TEK) with a permeation rate of 39 ng min^{-1} , which was
227 measured using UV optical absorption (Neuman et al., 2003). Solid or liquid samples of
228 oxalic (Sigma Aldrich, $\geq 99 \%$), butyric (Sigma Aldrich, $\geq 99 \%$), glycolic (Sigma Aldrich,
229 99%), propionic (Sigma Aldrich, $\geq 99.5 \%$) and valeric (Sigma Aldrich, $\geq 99 \%$) acids
230 were used in calibration measurements. The acid sample was placed in a glass impinger,
231 which was immersed in an ice bath to provide a constant vapor pressure. A flow of 6 to 10
232 mL min^{-1} of N_2 was passed over the organic acid in the glass impinger. This organic acid
233 air stream was then diluted with varying flows of N_2 (1 to 5 L min^{-1}) to achieve different
234 mixing ratios of the organic acid. Mixing ratios were calculated from either the acid's
235 emission rate from the impinger or the acid's vapor pressure. The emission rate of gas-
236 phase oxalic acid from the impinger was measured by scrubbing the output in deionized
237 water using the same method for calibrating the formic and acetic acid permeation tubes,
238 followed by ion chromatography analysis for oxalate. Three samples were analyzed and
239 the emission rate was determined to be 14 ng min^{-1} with a standard deviation of $< 5 \%$. The
240 vapor pressures of butyric and propionic acids at $0 \text{ }^\circ\text{C}$ were measured using a capacitance
241 manometer (MKS Instruments). The vapor pressures of glycolic and valeric acids at $0 \text{ }^\circ\text{C}$
242 were estimated using their literature vapor pressures at $25 \text{ }^\circ\text{C}$ and enthalpies of vaporization
243 (Daubert and Danner, 1989; Lide, 1995; Acree and Chickos, 2010).

244 Attempts to generate a calibration plot for pyruvic acid using its liquid sample
245 (Sigma Aldrich, 98 %) and the setup described above were unsuccessful as this acid was
246 found to interact very strongly with surfaces. Glyoxylic acid calibrations were not
247 performed due to the presence of impurities in the glyoxylic acid monohydrate solution
248 used (Sigma Aldrich, 98 %), which resulted in the appearance of ions not attributed to
249 glyoxylic acid. We attempted to generate calibration plots for malonic (Sigma Aldrich, \geq
250 99.5 %), succinic (Sigma Aldrich, 99 %) and glutaric (Sigma Aldrich, 99 %) acids by
251 passing N₂ over their solid samples at room temperature. However, it was not possible to
252 generate large enough gas phase concentrations for calibration since these organic acids
253 have very low vapor pressures. The vapor pressures of malonic, succinic and glutaric acids
254 are 5.73×10^{-4} , 1.13×10^{-4} and 4.21×10^{-4} kPa at 298 K, respectively (Booth et al., 2010),
255 which are at least 2 orders of magnitude lower than the organic acids that we calibrated.
256 Although heating up the malonic, succinic and glutaric acid samples will likely generate
257 sufficient vapors for calibration, this method of generating calibrant gases will lead to large
258 measurement uncertainties due to vapors condensing out and adhering onto surfaces at
259 room temperature prior to introduction into the CIMS.

260 **2.2.4. Detection limits and measurement uncertainties**

261 The detection limits of the organic acids were estimated as 3 times the standard
262 deviation values (3σ) of the ion signals measured during background mode. Although each
263 background measurement period lasted ~ 4 min, ion signals of the different organic acids
264 took up to 1.5 min to stabilize during the switch between ambient, calibration and
265 background measurements during the field study. Thus, ion signals measured during the
266 first 1.5 min were not included in the calculation of the average and standard deviation of
267 ion signals measured during background mode. Table 1 summarizes the average detection
268 limits of calibrated organic acids for 2.5 min averaging periods which corresponds to the
269 length of a background measurement with a 4 % duty cycle for each m/z. The mean
270 difference between successive background measurements ranged from 1 to 40 ppt for the
271 different organic acids. Future work will focus on reducing the instrument background, and
272 therefore improving the detection limits of these organic acids.

273 The uncertainties (1σ) in our ambient measurements of formic, acetic and oxalic
274 acid concentrations originated from CIMS and ion chromatography calibration
275 measurements. The ion chromatography measurement uncertainty was estimated to be 10
276 %. For formic and acetic acids, which were calibrated during the field study using
277 permeation tubes, their CIMS measurement uncertainties were estimated to be 6 and 7 %,
278 respectively, based on one standard deviation of the acids' calibrant ion signals. For oxalic
279 acid, which was calibrated in post-field laboratory work, the CIMS measurement
280 uncertainty was estimated to be 9 % based on one standard deviation of the $^{34}\text{SO}_2$
281 sensitivity (3 %), the acid's calibrant ion signals (7 %) and linear fit of the calibration curve
282 (5 %). Hence, the uncertainties in our ambient measurements of formic, acetic and oxalic
283 acid concentrations were estimated to be 12, 12 and 14 %, respectively.

284 For nitric acid, which was calibrated in post-field laboratory work using a
285 permeation tube and UV optical absorption, the uncertainty in its ambient concentrations
286 was estimated to be 13 % based on uncertainties in UV absorption measurements (10 %)
287 and one standard deviation of the acid's UV absorption signals (3 %), $^{34}\text{SO}_2$ sensitivity (3
288 %) and acid's calibrant ion signals (8 %). For propionic acid, which was calibrated in post-
289 field laboratory work using vapor pressures measured by a capacitance manometer, the
290 uncertainty in its ambient concentrations was estimated to be 14 % based on the vapor
291 pressure measurement uncertainty (10 %) and one standard deviation of the $^{34}\text{SO}_2$
292 sensitivity (3 %), the acid's calibrant ion signals (8 %) and linear fits of the acid's
293 calibration curves (3 %). Ambient concentrations and the corresponding uncertainties of
294 glycolic, valeric and butyric acids were not quantified.

295 **2.3. WSOC_g measurements**

296 WSOC_g was measured with a MIST chamber coupled to a total organic carbon
297 (TOC) analyzer (Sievers 900 series, GE Analytical Instruments). Ambient air first passed
298 through a Teflon filter (45 mm diameter, 2.0 μm pore size, Pall Life Sciences) to remove
299 particles in the air stream. This filter was changed every 3 to 4 days. The particle-free air
300 was then pulled into a glass Mist Chamber filled with ultrapure deionized water at a flow
301 rate of 20 L min^{-1} . The MIST chamber scrubbed soluble gases with Henry's law constants
302 greater than 10^3 M atm^{-1} into deionized water (Spaulding et al., 2002). The resulting liquid

303 samples from the MIST chamber were analyzed by the TOC analyzer. The TOC analyzer
304 converted the organic carbon in the liquid samples to carbon dioxide using UV light and
305 chemical oxidation. The carbon dioxide formed was then measured by conductivity. The
306 amount of organic carbon in the liquid samples is proportional to the measured increase in
307 conductivity of the dissolved carbon dioxide. Each WSOC_g measurement lasted 4 min.
308 Background WSOC_g measurements were performed for 45 min every 12 h by stopping the
309 sample air flow and rinsing the sampling lines with deionized water. The TOC analyzer
310 was calibrated using different concentrations of sucrose (as specified by the instrument
311 manual) before and after the field study. The limit of detection was 0.4 µgC m⁻³. The
312 measurement uncertainty was estimated to be 10 % based on uncertainties in the sample
313 air flow, liquid flow and TOC analyzer uncertainty. The MIST chamber and upstream
314 particle filter were located in an air-conditioned building so were generally below ambient
315 temperature. Hence, evaporation of collected particles (which will lead to positive artifacts
316 in WSOC_g measurements) are not expected to be significant.

317 **2.4. Supporting gas measurements**

318 Supporting gas measurements were provided by a suite of instruments operated by
319 the SEARCH network. A non-dispersive infrared spectrometer (Thermo Fisher Scientific)
320 provided hourly CO measurements. A UV absorption analyzer (Thermo Fisher Scientific)
321 provided hourly O₃ measurements. A gas chromatography-flame ionization detector (GC-
322 FID, Agilent Technologies) provided hourly VOC measurements.

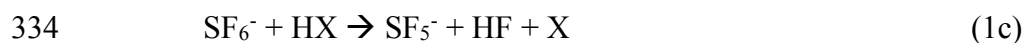
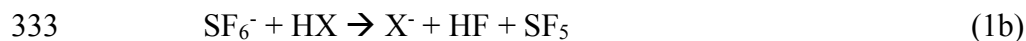
323 **3. Results and discussion**

324 **3.1. General SF₆⁻ CIMS field performance**

325 **3.1.1. SF₆⁻ ion chemistry with organic acids**

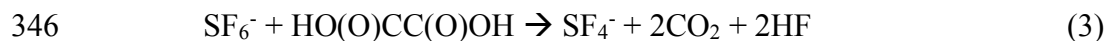
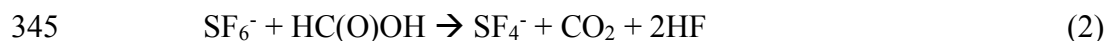
326 CIMS measurements of atmospheric constituents use ion-molecule reactions to
327 selectively ionize compounds of interest in the complex matrix of ambient air and produce
328 characteristic ions. The reactions of SF₆⁻ with the organic acids (HX) proceed through
329 reactions 1a to 1c, and gave similar products to those reported previously for SF₆⁻ reactions

330 with inorganic acids (Huey et al., 1995): SF₅⁻, X⁻ and X•HF where X⁻ is the conjugate base
331 of the organic acid (reactions 1a-c).



335 The effective branching ratios of the SF₅⁻, X⁻ and X•HF product ions can be impacted by
336 the field strength of the CDC. The SF₅⁻ ion (m/z 127, reaction 1c) is a common reaction
337 product of the reactions of SF₆⁻ with many species and is probably thermodynamically
338 driven by the formation of HF (Huey et al., 1995). Unfortunately, the production of SF₅⁻
339 does not allow for the selective detection of any atmospheric species. In addition, the larger
340 the branching ratio of the SF₅⁻ channel, the lower the CIMS sensitivity is to an individual
341 acid since the effective rate constants for the X⁻ and X•HF channels are lower.

342 The reaction of SF₆⁻ with formic acid and oxalic acid also produced SF₄⁻ ions (m/z
343 108). These reactions are probably thermodynamically driven by the formation of CO₂ and
344 HF:



347 We used the X⁻ and/or X•HF ions to determine ambient organic acid concentrations
348 since these ions are characteristic of the individual acids. For all the organic acids, the X⁻
349 •HF ion signal is substantially lower than that of the X⁻ ion for the conditions in this study.
350 However, this is probably largely due to the relatively high collision energy used in the
351 CDC, which led to efficient dissociation of the fluoride adducts to form X⁻ ions.
352 Consequently, only the proton transfer channel (1b) is used to quantify most of the organic
353 acids in the field study. The exceptions are formic and acetic acid as discussed in section
354 3.2.1 and 3.2.2

355 Table 1 shows a summary of the sensitivities of X⁻ and X•HF ions of some common
356 atmospheric organic acids. The average sensitivities of the HCOO⁻ (m/z 45) and HCOO⁻

357 •HF (m/z 65) ions of formic acid were 1.29 ± 0.22 and 0.29 ± 0.05 Hz ppt⁻¹, respectively,
358 while the average sensitivities of the CH₃COO⁻ (m/z 59) and CH₃COO•HF (m/z 79) ions
359 of acetic acid were 1.46 ± 0.29 and 0.30 ± 0.06 Hz ppt⁻¹, respectively. A weak ²¹⁰Po ion
360 source (< 1 mCi) was used by SF₆⁻-CIMS instrument during the field study, hence these
361 sensitivities will be substantially higher if a stronger radioactive source is used. Post-field
362 laboratory work suggest that the sensitivities may increase by as much as a factor of 5 for
363 a new commercial 20 mCi ²¹⁰Po ion source. Nevertheless, these sensitivities are compared
364 to formic and acetic acid sensitivities measured by a high-resolution time-of-flight
365 chemical ionization mass spectrometer (Aerodyne Research Inc.) that utilized I⁻ reagent
366 ions during the field study. Only the formic and acetic acid sensitivities were compared
367 since laboratory calibrations were not performed to determine the sensitivities for oxalic,
368 butyric, glycolic, propionic and valeric acids by I-CIMS. Although the formic acid
369 sensitivity measured by I-CIMS (1.33 ± 0.28 Hz ppt⁻¹) was comparable to that measured
370 by SF₆⁻-CIMS, the acetic acid sensitivity measured by I-CIMS (< 0.1 Hz ppt⁻¹) was
371 substantially lower than that measured by SF₆⁻-CIMS. Previous studies have similarly
372 reported low acetic acid sensitivity measured by I-CIMS (Aljawhary et al., 2013; Lee et
373 al., 2014).

374 Since many recent studies use I⁻ as a reagent ion to measure many compounds, the
375 measured SF₆⁻ sensitivities to organic acids are compared with those of I⁻ reported by Lee
376 et al. (2014, 2018). However, it is important to note that the absolute SF₆⁻ and I⁻ sensitivities
377 values are specific to the respective instruments and their configuration. The sensitivity to
378 individual compounds depend on a variety of instrument parameters (e.g., flow rates,
379 pressures, electric fields, ion source activity) that control ion production and transmission,
380 reaction time, declustering efficiency, etc. Consequently, this analysis serves primarily as
381 a qualitative comparison of SF₆⁻ and I⁻ sensitivity.

382 Although the I⁻ sensitivity to formic acid (2.9 Hz ppt⁻¹) reported by Lee et al. (2014)
383 is higher than that of SF₆⁻ (1.29 Hz ppt⁻¹), the SF₆⁻ sensitivities for the other organic acids
384 (i.e., acetic, oxalic, glycolic and propionic acids) are substantially higher than those of I⁻
385 (Table S1a). The SF₆⁻ CIMS method is particularly sensitive to oxalic, propionic and
386 glycolic acids, which are expected to be present at low concentrations in the atmosphere.

387 The sensitivities of SF_6^- and I^- to SO_2 , HNO_3 and HCl can also be compared (Table S1b).
388 The SF_6^- sensitivities of SO_2 and HCl are significantly higher than that of I^- reported by
389 Lee et al. (2018). However, I^- is more sensitive to HNO_3 .

390 3.1.2. Characterization of interferences

391 SF_6^- is very sensitive to many trace atmospheric species but its reactions with water
392 vapor and O_3 when sampling ambient air can lead to issues both with selectivity and
393 stability. For example, SF_6^- reacts nonlinearly with water vapor to form a series of $\text{F}^-\cdot(\text{HF})_n$
394 cluster ions (Huey et al., 1995; Arnold and Viggiano, 2001). SF_6^- also reacts efficiently
395 with O_3 to form O_3^- , which is rapidly converted to CO_3^- in ambient air (Slusher et al., 2001).
396 These reactions can deplete SF_6^- as well as form a variety of potentially interfering ions
397 from secondary reactions (e.g., $\text{F}^-\cdot(\text{HF})_n$ and CO_3^- ions) that depend on more abundant
398 atmospheric species. For these reasons, efforts were made to minimize interferences by
399 limiting reaction times and the flow sampled into the CIMS. This was accomplished by
400 sampling only 0.3 L min^{-1} of air through the variable orifice into the flow tube and
401 maintaining the flow tube at a low pressure ($\sim 13 \text{ mbar}$). The 0.3 L min^{-1} sampled air flow
402 is diluted by 3.7 slpm of N_2/SF_6 flow in the flow tube. The ratio of the sampled air flow to
403 the N_2/SF_6 flow introduced into the flow tube is approximately 1:13. While the high N_2/SF_6
404 flow (3.7 slpm) passed through the radioactive source into the flow tube increased the SF_6^-
405 reagent ion signal, the high dilution of the sampled air flow in the flow tube reduced the
406 CIMS instrument sensitivity by decreasing the number density of the analytes.

407 Figure 2 shows a mass spectrum of ambient air. Interference peaks at m/z 39 ($\text{F}^-\cdot(\text{HF})$
408 and CO_3^- , respectively) can be attributed to the presence of water and O_3 ,
409 respectively. The reagent ion $^{32}\text{SF}_6^-$ is present at m/z 146. The $^{32}\text{SF}_6^-$ reagent ion signal was
410 saturated, and this caused the sharp drop in the m/z 146 signal as shown in Fig. 2. Since
411 the $^{32}\text{SF}_6^-$ reagent ion signal was saturated for the entire field study, we monitored the ion
412 signal of its isotope $^{34}\text{SF}_6^-$ to determine if the reaction of SF_6^- with ambient water vapor
413 (5.92×10^{-6} to $2.19 \times 10^{-5} \text{ g cm}^{-3}$) and O_3 (2.1 to 82.4 ppb) depleted SF_6^- reagent ions.
414 Figure S2a shows the time series of the $^{34}\text{SF}_6^-$ ion signal and ambient water vapor
415 concentration for the entire field study. Despite fluctuations in ambient water vapor and O_3
416 concentrations, the $^{34}\text{SF}_6^-$ ion signal was relatively constant for the entire field study with

417 a standard deviation of < 3%. This indicates that the reaction of SF_6^- with ambient water
418 vapor and O_3 did not significantly deplete the $^{32}\text{SF}_6^-$ reagent ions during the field study.

419 The $\text{F}_2^{34}\text{SO}_2^-$ ion signal was used to monitor the CIMS SO_2 sensitivity during the
420 field study. Figure S2b shows the time series of the $\text{F}_2^{34}\text{SO}_2^-/^{34}\text{SF}_6^-$ ion signal ratio obtained
421 in calibration measurements. There is a ~50 % increase in the $\text{F}_2^{34}\text{SO}_2^-/^{34}\text{SF}_6^-$ ion signal
422 ratio on 28 Sept 2016, indicating an increase in the CIMS instrument sensitivity. The
423 increase in CIMS instrument sensitivity is due to the decrease in ambient water vapor
424 concentrations on 28 Sept 2016 (Fig. S2a). Previous laboratory and field studies showed
425 that this was due to the hydrolysis of $\text{F}_2^{34}\text{SO}_2^-$, which led to the loss of this ion and
426 diminished sensitivity at higher levels of ambient water vapor (Arnold and Viggiano, 2001;
427 Slusher et al., 2001). However, the SO_2 sensitivity at $\text{F}_2^{34}\text{SO}_2^-$ only varied within a factor
428 of two for the entire field study with a clear relationship to water vapor (Fig. S2c). The SO_2
429 sensitivity did not show any obvious dependence on ambient O_3 concentrations (Fig. S2d).

430 The formic (HCOO^- at m/z 45 and $\text{HCOO}\cdot\text{HF}$ at m/z 65) and acetic (CH_3COO^-
431 $\cdot\text{HF}$ at m/z 79) acid ions did not show any obvious dependence on ambient water vapor
432 and O_3 concentrations during calibration measurements (Fig. S3). Therefore, we do not
433 expect the sensitivities of the X^- and $\text{X}\cdot\text{HF}$ ions of the studied organic acids to depend on
434 ambient water vapor and O_3 concentrations. We accounted for water vapor dependence of
435 the $\text{F}_2^{34}\text{SO}_2^-$ ion signal using the linear relationship between the $\text{F}_2^{34}\text{SO}_2^-$ ion sensitivity
436 and ambient water vapor concentration (Fig. S2c) in our post-field calibrations, where the
437 response of the CIMS acid signals were measured relative to the of the $^{34}\text{SO}_2$ sensitivity.

438 3.1.3. Background and calibration measurements

439 Figure S4 shows an example of the CIMS instrument response during the switch
440 between background, calibration and ambient measurements of formic and acetic acids
441 during the field study. The 13 s time resolution data was used to determine the CIMS
442 instrument time response. Formic (m/z 45, 65 and 108) and acetic (m/z 79) acid ion signals
443 took ~1.5 min to reach a steady state after switches between ambient, calibration and
444 background measurements (Figs. S4a and S4c).

445 The CIMS time response to a compound is governed primarily by the compound's
446 propensity to adhere to surfaces. The decays in the formic and acetic acid ion signals and
447 times required for them to reach steady state after the removal of calibration gases during
448 the switch from standard addition calibration to ambient sampling were used to determine
449 the CIMS response time. The signal decays were fitted using double exponential functions.
450 For formic acid, the m/z 45, 65 and 108 ion signals decayed to $1/e^2$ in 37 ± 2 , 33 ± 2 and
451 32 ± 2 s, respectively (Fig. S4b). For acetic acid, the m/z 79 ion signal decayed to $1/e^2$ in
452 42 ± 2 s (Fig. S4d).

453 **3.2. Ambient measurements**

454 **3.2.1. Formic acid**

455 Figure 2 shows typical mass spectra obtained under background and measurement
456 modes during the field study. The SF_6^- reagent ion is present at m/z 146. One of the
457 prominent species in the mass spectrum is formic acid, which is detected as HCOO^- and
458 $\text{HCOO}\cdot\text{HF}$ at m/z 45 and 65, respectively. Our laboratory studies demonstrated that the
459 reaction of formic acid with SF_6^- also produced a large fraction of SF_4^- ions at m/z 108.
460 The reaction of SF_6^- with oxalic acid also produced SF_4^- ions, but its SF_4^- product ion yield
461 is low and gas phase oxalic acid is not present in large concentrations. In addition, SF_4^- is
462 present in the mass spectrum obtained under background mode but the SF_4^- background
463 ion signals are lower than those typically observed in measurement mode at the Yorkville
464 site. As a result, we determined the ambient formic acid concentrations using the HCOO^- ,
465 $\text{HCOO}\cdot\text{HF}$ and SF_4^- ions. Figure 3a shows a scatter plot comparing the ambient formic
466 acid concentrations measured at Yorkville using the HCOO^- , $\text{HCOO}\cdot\text{HF}$ and SF_4^- ions.
467 Linear regression analysis reveals that the formic acid concentrations determined by the
468 three ions are highly correlated ($R^2 = 0.99$) with slopes exhibiting a near 1:1 correlation.
469 The excellent correlation between these three ions and the agreement with laboratory data
470 indicates that formic acid is selectively measured by this method.

471 The time series of formic acid, temperature and solar radiation measured at
472 Yorkville are shown in Fig. 3b. Formic acid concentrations ranged from 40 ppt to 4 ppb
473 during the field study, with strong and consistent diurnal trends. The day-to-day variability

474 in formic acid concentrations are associated with changes in solar radiation and
475 temperature. Higher formic acid concentrations are measured during warm and sunny days,
476 similar to formic acid measurements performed in Centreville, rural Alabama during the
477 2013 Southern Oxidant Aerosol Study (SOAS) (Brophy and Farmer, 2015; Millet et al.,
478 2015). Figure 3c shows the study-averaged diurnal profiles of formic acid and solar
479 irradiance. Formic acid started to increase at 7:30, which coincided with a sharp increase
480 in solar irradiance. Concentrations continued to increase throughout the day and peaked at
481 18:30, which coincided with the approximate time just before solar irradiance reached zero.
482 Formic acid then decreased continuously throughout the night.

483 The immediate early-morning increase in formic acid observed in this field study
484 is similar to that seen during the SOAS study (Millet et al., 2015). However, there are some
485 differences in the formic acid diurnal cycles measured in this field study and the SOAS
486 study. Formic acid peaked at 15:30 during SOAS, approximately 3 hours before solar
487 irradiance decreased to zero. In contrast, formic acid concentrations only started to
488 decrease at sunset (at 19:30) in this study. This suggests that there may be differences in
489 the types and/or magnitudes of formic acid sources and sinks in this two field studies. Land
490 cover and/or land use differences may have contributed to differences in formic acid
491 sources and sinks at the Centreville and Yorkville field sites. The area surrounding the
492 Yorkville field site is covered primarily by hardwood mixed with farmland and open
493 pastures. In contrast, the Centreville field site is surrounded by forests comprised of mixed
494 oak-hickory and loblolly trees (Hansen et al., 2003). It is also possible that seasonal
495 differences contributed to differences in formic acid sources and sinks in the two field
496 studies. The SOAS campaign took place in the middle of summer (1 June to 15 July 2013)
497 when biogenic emissions are typically higher while this field study took place in early fall
498 when biogenic emissions are lower due to cooler temperatures. For example, the average
499 concentration of isoprene (a formic acid source) in this study (1.21 ppb) is lower than that
500 in SOAS (1.92 ppb (Millet et al., 2015)). Despite these differences, our overall results are
501 similar to the formic acid measurements performed in SOAS in both magnitude and diurnal
502 variability.

503 **3.2.2. Acetic acid**

504 Acetic acid is detected with SF_6^- as CH_3COO^- and $\text{CH}_3\text{COO}^-\cdot\text{HF}$ at m/z 59 and 79,
505 respectively. However, these ions are subject to interferences from the reaction of SF_6^- with
506 water vapor present in the sampled ambient air. Two of these interfering ions $\text{F}^-\cdot(\text{HF})_2$ and
507 $\text{F}^-\cdot(\text{HF})_3$ occur at m/z 59 and 79, respectively. As discussed earlier, we minimized the
508 impact of these interferences by diluting the sample flow into the CIMS and running the
509 CDC at a high collision energy to dissociate the HF cluster ions. As expected from cluster
510 bond strengths, we found that larger HF cluster ions dissociated more easily than smaller
511 ones. For example, at a CDC electric field of $\sim 113 \text{ V cm}^{-1}$ (the configuration used in this
512 field study), virtually all of the $\text{F}^-\cdot(\text{HF})_3$ cluster ions dissociated while very few of the $\text{F}^-\cdot$
513 $\cdot(\text{HF})$ cluster ions dissociated. This indicates that the m/z 79 channel for acetic acid is more
514 immune to interference from water vapor than the m/z 59 channel. This is supported by the
515 observation that the background ion signal at m/z 59 ($R^2 = 0.50$) is more highly correlated
516 with ambient water vapor concentrations than the background ion signal of m/z 79 ($R^2 =$
517 0.30). In addition, the m/z 59 ion is subjected to interference from the reaction of SF_6^- with
518 O_3 present in the sampled ambient air. SF_6^- reacts with O_3 in the presence of CO_2 to form
519 CO_3^- at m/z 60 (Slusher et al., 2001). As shown in Fig. 2, the large CO_3^- peak at m/z 60 is
520 a potential interference to the m/z 59 signal. As the background scrubber also removed O_3
521 from the ambient air, there is a large difference in the m/z 60 ion signal between the
522 measurement and background modes ($\sim 100\,000 \text{ Hz}$). Thus, even a few percent bleed over
523 of m/z 60 to m/z 59 can lead to an over-estimation of ambient acetic acid concentrations.
524 For these reasons, we used m/z 79 ($\text{X}^-\cdot\text{HF}$) to determine ambient acetic acid concentrations
525 even though this channel has a lower sensitivity than the m/z 59 channel (X^-).

526 The time series of acetic acid, temperature and solar radiation measured at
527 Yorkville are shown in Fig. 4a. Acetic acid concentrations ranged from 30 ppt to 3 ppb
528 during the field study. The day-to-day variability in acetic acid concentrations resembled
529 the behavior of formic acid concentrations, with higher concentrations being measured
530 during warm and sunny days. Figure 4b shows the study-averaged diurnal profiles of acetic
531 acid and solar irradiance. The diurnal profile of acetic acid is similar to that of formic acid
532 with a more pronounced evening maximum. Acetic acid started to increase at 7:30 and
533 built up through the day, peaking at 19:30 and decreased continuously overnight. In
534 general, acetic acid concentrations are well correlated with ($R^2 = 0.67$) and comparable in

535 magnitude (~60 % on average) to formic acid. The study-averaged formic acid/acetic acid
536 concentration ratio (1.65) is comparable to ratios from previous field studies in rural and
537 urban environments (Talbot et al., 1988; Talbot et al., 1995; Granby et al., 1997; Khare et
538 al., 1999; Talbot et al., 1999; Baboukas et al., 2000; Singh et al., 2000; Kuhn et al., 2002;
539 Baasandorj et al., 2015; Millet et al., 2015).

540 **3.2.3. Larger organic acids**

541 In addition to formic and acetic acid, eight other ions were monitored during the
542 field study: m/z 73, 75, 87, 89, 101, 103, 117 and 131. These ions were chosen as they had
543 significant signals when ambient air was sampled and were not obviously formed from
544 SF_6^- reaction with water vapor or O_3 . Since the CIMS utilized in this study only had unit
545 mass resolution, these ions are the sum of all organic acid isomers and isobaric organic
546 acids of the same molecular weight as well as other product ions from species that might
547 react with SF_6^- . We will refer to organic acids with m/z 75, 87, 101, 103, 117 and 131 by
548 their ion masses. We assign the m/z 73 ion as the X^- ion of propionic acid because it does
549 not have organic acid isomers and isobaric species at that m/z . In addition, real-time ion
550 chromatography measurements of aerosol composition performed during the field study
551 demonstrated the presence of particulate oxalic acid (Nah et al., 2018). For this reason, we
552 assign the m/z 89 ion as the X^- ion of oxalic acid. As shown in Nah et al. (2018), the gas-
553 particle ratios of the organic acids depend of their thermodynamic conditions, which are
554 dependent on the acid's physicochemical properties, ambient temperature, particle water
555 and pH. Since the measured gas-particle partitioning ratios of oxalic acid (calculated using
556 the CIMS and ion chromatography measurements) are in good agreement with their
557 corresponding thermodynamic predictions (Nah et al., 2018), this indicated that our
558 assignment of the m/z 89 ion to oxalic acid is reasonable. In addition, the high sensitivity
559 of SF_6^- to oxalic acid also helps limit interferences due to other acids. Particulate formic
560 acid and acetic acid were also detected by ion chromatography during the field study, but
561 were at much lower concentrations relative to the gas phase (Nah et al., 2018).

562 Figures 5 and S5 show the time series and diurnal profiles of oxalic and propionic
563 acids and organic acids with ions m/z 75, 87, 101, 103, 117 and 131 measured during the
564 field study. These organic acids displayed very similar day-to-day variability as formic and

565 acetic acids, with higher concentrations (or ion signals) being measured on warm and sunny
566 days. The diurnal profiles of all the measured organic acids have similar diurnal trends,
567 with their concentrations (or ion signals) reaching a maximum between 17:30 and 19:30
568 and rapidly decreasing after sunset.

569 **3.2.4. Comparison with WSOC_g**

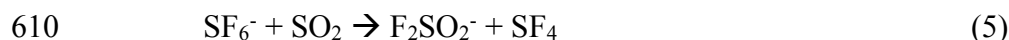
570 WSOC_g measurements were performed during the field study using a MIST
571 chamber coupled to a TOC analyzer. The study average WSOC_g was $3.6 \pm 2.7 \mu\text{gC m}^{-3}$,
572 slightly lower than that measured during the SOAS study ($4.9 \mu\text{gC m}^{-3}$) (Xu et al., 2017),
573 and approximately four times lower than that measured in urban Atlanta, Georgia (13.7
574 $\mu\text{gC m}^{-3}$) (Hennigan et al., 2009). Despite being comparable in magnitude, the diurnal
575 profiles of WSOC_g measured in this study and the SOAS study are different. WSOC_g
576 measured in the SOAS study decreased at sunset, while WSOC_g measured in this study
577 decreased 2 hours after sunset. Differences in WSOC_g concentrations and diurnal profiles
578 at the three different sites may be due to differences in emission sources as a result of
579 different measurement periods, land use and/or land cover.

580 To estimate the fraction of WSOC_g that is comprised of organic acids, the total
581 organic carbon contributed by formic, acetic, oxalic and propionic acids is compared to the
582 WSOC_g measurements. This comparison primarily serves as a check to determine if the
583 peak assignments are plausible by ensuring that the estimated sum of organic carbon
584 contributed by these four organic acids is less than or equal to the measured WSOC_g.
585 Figures 6a and 6b show the time series and diurnal profiles of WSOC_g and the organic
586 carbon contributed by the four organic acids. Formic and acetic acids comprised majority
587 of the total organic carbon contributed by the four organic acids (study averages of 41 and
588 54 %, respectively). The carbon mass fraction of WSOC_g comprised of these four organic
589 acids ranged from 2 to 100 %. Based on the orthogonal distance regression slope shown in
590 Fig. 6c, the study-averaged carbon mass fraction of WSOC_g comprised of the four organic
591 acids is 22 %. The total organic carbon contributed by the four organic acids are moderately
592 correlated with WSOC_g ($R^2 = 0.42$). This is likely due to the presence of other water-soluble
593 gas phase species (with different day-to-day variability from the organic acids) that
594 contribute to the WSOC_g. This is supported by slight differences in the diurnal profiles of

595 WSOC_g and the organic carbon contributed by the organic acids (Fig. 6b). While the
596 diurnal profiles of WSOC_g and the organic carbon contributed by the four organic acids
597 have similar general shapes, WSOC_g peaked at 21:30, approximately 2 hours after the solar
598 irradiance have decreased to zero. In contrast, the organic carbon contributed by the four
599 organic acids start to decrease at sunset (at 19:30).

600 3.2.5. SO₂ and HNO₃ observations

601 In addition to evaluating the field performance of the SF₆⁻ CIMS technique in gas-
602 phase organic acid measurements, another focus of this study was to investigate the
603 possible sources of the measured organic acids. For this reason, HNO₃ and SO₂ (two
604 common anthropogenic tracers) were also measured by SF₆⁻ CIMS during the field study.
605 Correlations between the concentrations of organic acids and those of HNO₃ and SO₂ were
606 then examined to determine if the organic acids were anthropogenic in nature (section 3.3).
607 While their reactions with SF₆⁻ have multiple product channels (Huey et al., 1995), only
608 the NO₃⁻•HF (m/z 82) and F₂SO₂⁻ (m/z 102) ions were used for quantitative purposes:



611 Figure S6 shows the time series of SO₂ and HNO₃ measured during the field study.
612 As expected at a rural site, SO₂ and HNO₃ concentrations are low most of the time (study
613 averages of 230 and 180 ppt, respectively). However, there were occasional periods when
614 the site was impacted by anthropogenic pollution. In particular, there are spikes in both
615 SO₂ and HNO₃ concentrations lasting between 1 to 3 hours throughout the study that
616 corresponded to the site being impacted by power plant or urban emissions. Outside of
617 these anthropogenic spikes, HNO₃ showed a clear diurnal profile with a maximum at
618 approximately 12:30, consistent with local photochemical production.

619 3.3. Potential sources of organic acids

620 Correlation analysis on organic acid concentrations can provide insights on their
621 sources. Figure 7 shows that the concentration of formic acid is strongly correlated with
622 those of the other measured organic acids (R² = 0.68 to 0.89). This suggests that these

623 organic acids have the same or similar sources at Yorkville. The sources of organic acids
624 can be biogenic or anthropogenic in nature. To determine if the primary sources of organic
625 acids are of biogenic or anthropogenic origin, we first examined the correlations of organic
626 acid concentrations with those of anthropogenic pollutants CO, SO₂, O₃ and HNO₃. CO
627 and SO₂ are common tracers for combustion sources. The organic acid concentrations (or
628 ion signals) are poorly correlated with CO (Fig. S7, R² = 0.04 to 0.15) and SO₂ (Fig. S8,
629 R² = 0.01 to 0.23), indicating that primary emissions from combustion are a minor source
630 of organic acids in Yorkville. HNO₃ and O₃ are common photochemical tracers of urban
631 air masses. The organic acid concentrations (or ion signals) are weakly correlated with O₃
632 (Fig. S9, R² = 0.11 to 0.31) and HNO₃ (Fig. S10, R² = 0.33 to 0.60). In addition, there is
633 no noticeable increase in organic acid concentrations during periods of elevated CO, SO₂,
634 O₃ and HNO₃ concentrations when the site was impacted by pollution plumes. Formic
635 acid/CO ratios (which have been used in some studies to determine the contribution of
636 polluted air masses) ranged between 1.0 x 10⁻³ to 2.5 x10⁻² ppb ppb⁻¹. The ratio peaked
637 consistently in the mid-afternoon, which coincided with when formic acid and CO reached
638 their maximum and minimum, respectively. In addition, there were no spikes in the formic
639 acid/CO ratio during the study, suggesting that contributions of polluted air masses to the
640 daily increase in formic acid are minimal. Together, these results indicate that the primary
641 sources of organic acids in Yorkville are likely not anthropogenic in nature.

642 Diurnal profiles of the measured organic acids suggest that their sources are linked
643 to higher daytime temperatures and/or photochemical processes. Figure 8 compares the
644 concentrations (or ion signals) of organic acids against ambient temperatures measured
645 during the study. Since there was a noticeable decrease in mean ambient temperatures
646 starting on 28 Sept 2016, we grouped the datasets into two time periods (3 to 27 Sept and
647 28 Sept to 12 Oct) to better evaluate the effect of temperature on organic acid
648 concentrations. The average temperature in the first time period (3 to 27 Sept) is 24.8 °C
649 (32.6 °C max, 18.1 °C min), while the average temperature in the second time period (28
650 Sept to 12 Oct) is 19.5 °C (28.4 °C max, 9.5 °C min). We find that organic acid
651 concentrations are on average higher and more highly correlated with temperatures in the
652 warmer first time period (R² = 0.40 to 0.61) compared to the cooler second time period (R²

653 = 0.18 to 0.55). These observations can be explained by temperature-dependent emissions
654 of organic acids and their BVOC precursors. Previous studies have shown that emissions
655 of organic acids and their BVOC precursors depend strongly on light and temperature, with
656 substantially lower concentrations being emitted in the dark and/or at low temperatures
657 (Kesselmeier et al., 1997; Kesselmeier, 2001; Sindelarova et al., 2014). We find that the
658 concentration of isoprene, which was the dominant BVOC in Yorkville, has a somewhat
659 similar diurnal profile as the organic acids and decreased with temperature on 28 Sept 2016
660 (Fig. S11). In addition, the concentrations of formic and acetic acids are moderately
661 correlated with that of isoprene ($R^2 = 0.42$ and 0.40 , respectively) (Fig. S12).

662 Multiphase photochemical aging of ambient organic aerosols can also be a source
663 of gas-phase organic acids (Eliason et al., 2003; Ervens et al., 2004; Molina et al., 2004;
664 Lim et al., 2005; Park et al., 2006; Walser et al., 2007; Sorooshian et al., 2007; Vlasenko
665 et al., 2008; Pan et al., 2009; Sorooshian et al., 2010). Organic acids may be formed in the
666 particle phase during organic aerosol photochemical aging, with subsequent volatilization
667 into the gas phase. Real-time ion chromatography measurements of aerosol composition
668 demonstrated the presence of particulate formic, acetic, oxalic, malonic, succinic and
669 glutaric acids (Nah et al., 2018). However, since the ratios of gas-phase formic and acetic
670 acid mass concentration to the total organic aerosol mass concentration are large (study
671 averages of 40 and 35 %, respectively) (Nah et al., 2018), it is unlikely that organic aerosol
672 photochemical aging is a large source of formic and acetic acids. In contrast, the ratios of
673 gas-phase oxalic, malonic, succinic and glutaric acids mass concentration to the total
674 organic aerosol mass concentration are expected to be small, suggesting that organic
675 aerosol photochemical aging may be an important source of these gas-phase organic acids.

676 In summary, the temperature dependence and diurnal profile of organic acid
677 concentrations combined with poor correlations between organic acid concentrations and
678 those of anthropogenic pollutants CO, SO₂, O₃ and HNO₃ strongly suggest that the primary
679 sources of gas-phase organic acids at Yorkville are biogenic in nature. However, our data
680 alone does not allow us to determine if the organic acids are a result of direct emissions or
681 photochemical oxidation of other BVOC emissions and/or organic aerosols. Partitioning

682 of these organic acids between the gas and particle phases is discussed in another paper
683 (Nah et al., 2018).

684 **4. Summary**

685 SF_6^- reacted with all of the studied organic acids to produce product ions that were
686 characteristic of the individual acids (i.e., X^- or $\text{X}\cdot\text{HF}$). These reactions all occurred at less
687 than the maximum collisional rate due to significant yields of SF_5^- and SF_4^- , which reduced
688 the sensitivity of the method. For the conditions employed in this study, the sensitivities of
689 X^- and $\text{X}\cdot\text{HF}$ ions of the organic acids ranged from 0.12 to 6.38 Hz ppt⁻¹. The detection
690 limits of the organic acids were approximated from 3 times the standard deviation values
691 (3σ) of the ion signals obtained during background measurements. Limits of detection
692 ranged from 1 to 60 ppt for 2.5 min integration periods for the organic acids studied. It
693 should be noted that the SF_6^- CIMS method is particularly sensitive to oxalic, propionic
694 and glycolic acids, which are expected to be present at low concentrations in the
695 atmosphere. Water vapor and O_3 can lead to interferences with this method but for the
696 conditions employed in this study, they were largely limited to acetic acid measurements
697 at m/z 59. However, fluctuations in ambient water vapor can also lead to changes in
698 sensitivity for the detection of some species (e.g., SO_2). Uncertainties in organic acid
699 concentrations originate primarily from calibration measurements and ranged from 12 to
700 14 %. Overall, the tractable mass spectra obtained by the SF_6^- CIMS method coupled with
701 reasonable limits of detection and the high correlations observed between the individual
702 organic acids demonstrated the potential of this method. Obvious next steps for the SF_6^-
703 CIMS method are to compare it to other measurement methods for organic acids and to
704 deploy the SF_6^- ion chemistry to a higher resolution time-of-flight mass spectrometer to
705 reduce the potential for interferences.

706 The SF_6^- CIMS method was deployed for measurements of gas phase organic acids
707 in a mixed forest-agricultural area in Yorkville, Georgia from Sept to Oct 2016. The
708 organic acids measured in the field study were formic, acetic, propionic and oxalic acids.
709 Ambient concentrations of these organic acids ranged from a few ppt to several ppb. All
710 the organic acids exhibited similar strong diurnal trends. Organic acid concentrations built
711 up throughout the day, peaked between 17:30 and 19:30 before decreasing continuously

712 overnight. Strong correlations between organic acid concentrations indicated that these
713 organic acids likely have the same or similar sources at Yorkville. We concluded that the
714 organic acids were likely not due to anthropogenic emissions since they were poorly
715 correlated with anthropogenic pollutants and their concentrations were not elevated when
716 the site was impacted by pollution plumes. Higher organic acid concentrations were
717 measured during warm and sunny days. Organic acid concentrations were strongly
718 correlated with temperature during the first month of the study when ambient temperatures
719 were high. Together, our results suggested that the primary sources of organic acids at
720 Yorkville were biogenic in nature. Direct biogenic emissions of organic acids and/or their
721 BVOC precursors were likely enhanced at high ambient temperatures, resulting in the
722 observed variability of organic acid concentrations. Another potential source is the
723 production of organic acids in the particle phase from the multiphase photochemical aging
724 of organic aerosols followed by evaporation to the gas phase, though this source is likely
725 not a large source of formic and acetic acids. However, given the inability of current models
726 and photochemical mechanisms to explain formic acid observations in the Southeastern
727 U.S. (Millet et al., 2015), it is unlikely that our observations of formic acid and larger
728 organic acids can be explained as well. Further work (i.e., laboratory, field and modeling
729 studies) is needed to determine how organic acids are formed in the atmosphere.

730 **5. Acknowledgements**

731 The authors thank Eric Edgerton (Atmospheric Research and Analysis, Inc.) for
732 providing CO, O₃ and VOC measurements and meteorological data. We also thank Young
733 Ro Lee for performing laboratory experiments to determine SF₆⁻ sensitivity to HCl.

734 **6. Funding**

735 This publication was developed under US Environmental Protection Agency (EPA)
736 STAR Grant R835882 awarded to Georgia Institute of Technology. It has not been
737 formally reviewed by the EPA. The views expressed in this document are solely those of
738 the authors and do not necessarily reflect those of the EPA. EPA does not endorse any
739 products or commercial services mentioned in this publication.

740 **7. Competing financial interests**

741 The authors declare no competing financial interests.

742 **8. Data availability**

743 Data can be accessed by request (greg.huey@eas.gatech.edu).

744 **9. References**

745 Acree, W., and Chickos, J. S.: Phase Transition Enthalpy Measurements of Organic and
746 Organometallic Compounds. Sublimation, Vaporization and Fusion Enthalpies From 1880
747 to 2010, *J. Phys. Chem. Ref. Data*, 39, 942, 10.1063/1.3309507, 2010.

748 Aljawhary, D., Lee, A. K. Y., and Abbatt, J. P. D.: High-resolution chemical ionization
749 mass spectrometry (ToF-CIMS): application to study SOA composition and processing,
750 *Atmospheric Measurement Techniques*, 6, 3211-3224, 10.5194/amt-6-3211-2013, 2013.

751 Andreae, M. O., Talbot, R. W., Andreae, T. W., and Harriss, R. C.: Formic and Acetic
752 Acid over the Central Amazon Region, Brazil. 1. Dry Season, *Journal of Geophysical
753 Research-Atmospheres*, 93, 1616-1624, 10.1029/JD093iD02p01616, 1988.

754 Arnold, S. T., and Viggiano, A. A.: Turbulent ion flow tube study of the cluster-mediated
755 reactions of SF₆⁻ with H₂O, CH₃OH, and C₂H₅OH from 50 to 500 torr, *J. Phys. Chem.
756 A*, 105, 3527-3531, 10.1021/jp003967y, 2001.

757 Baasandorj, M., Millet, D. B., Hu, L., Mitroo, D., and Williams, B. J.: Measuring acetic
758 and formic acid by proton-transfer-reaction mass spectrometry: sensitivity, humidity
759 dependence, and quantifying interferences, *Atmospheric Measurement Techniques*, 8,
760 1303-1321, 10.5194/amt-8-1303-2015, 2015.

761 Baboukas, E. D., Kanakidou, M., and Mihalopoulos, N.: Carboxylic acids in gas and
762 particulate phase above the Atlantic Ocean, *Journal of Geophysical Research-
763 Atmospheres*, 105, 14459-14471, 10.1029/1999jd900977, 2000.

764 Booth, A. M., Barley, M. H., Topping, D. O., McFiggans, G., Garforth, A., and Percival,
765 C. J.: Solid state and sub-cooled liquid vapour pressures of substituted dicarboxylic acids

766 using Knudsen Effusion Mass Spectrometry (KEMS) and Differential Scanning
767 Calorimetry, *Atmos. Chem. Phys.*, 10, 4879-4892, 10.5194/acp-10-4879-2010, 2010.

768 Brophy, P., and Farmer, D. K.: A switchable reagent ion high resolution time-of-flight
769 chemical ionization mass spectrometer for real-time measurement of gas phase oxidized
770 species: characterization from the 2013 southern oxidant and aerosol study, *Atmospheric
771 Measurement Techniques*, 8, 2945-2959, 10.5194/amt-8-2945-2015, 2015.

772 Carlton, A. G., Turpin, B. J., Lim, H. J., Altieri, K. E., and Seitzinger, S.: Link between
773 isoprene and secondary organic aerosol (SOA): Pyruvic acid oxidation yields low volatility
774 organic acids in clouds, *Geophys. Res. Lett.*, 33, 4, 10.1029/2005gl025374, 2006.

775 Chebbi, A., and Carlier, P.: Carboxylic acids in the troposphere, occurrence, sources, and
776 sinks: A review, *Atmospheric Environment*, 30, 4233-4249, 10.1016/1352-
777 2310(96)00102-1, 1996.

778 Crounse, J. D., McKinney, K. A., Kwan, A. J., and Wennberg, P. O.: Measurement of gas-
779 phase hydroperoxides by chemical ionization mass spectrometry, *Analytical Chemistry*,
780 78, 6726-6732, 10.1021/ac0604235, 2006.

781 Daubert, T. E., and Danner, R. P.: Physical and thermodynamic properties of pure
782 chemicals: data compilation, Taylor & Francis, Washington, DC, 1989.

783 Eliason, T. L., Aloisio, S., Donaldson, D. J., Cziczo, D. J., and Vaida, V.: Processing of
784 unsaturated organic acid films and aerosols by ozone, *Atmospheric Environment*, 37, 2207-
785 2219, 10.1016/s1352-2310(03)00149-3, 2003.

786 Ervens, B., Feingold, G., Frost, G. J., and Kreidenweis, S. M.: A modeling study of aqueous
787 production of dicarboxylic acids: 1. Chemical pathways and speciated organic mass
788 production, *Journal of Geophysical Research-Atmospheres*, 109, 10.1029/2003jd004387,
789 2004.

790 Ervens, B., Carlton, A. G., Turpin, B. J., Altieri, K. E., Kreidenweis, S. M., and Feingold,
791 G.: Secondary organic aerosol yields from cloud-processing of isoprene oxidation
792 products, *Geophys. Res. Lett.*, 35, 10.1029/2007gl031828, 2008.

793 Galloway, J. N., Likens, G. E., Keene, W. C., and Miller, J. M.: The Composition of
794 Precipitation in Remote Areas of the World, *Journal of Geophysical Research-Oceans and*
795 *Atmospheres*, 87, 8771-8786, 10.1029/JC087iC11p08771, 1982.

796 Granby, K., Egelov, A. H., Nielsen, T., and Lohse, C.: Carboxylic acids: Seasonal variation
797 and relation to chemical and meteorological parameters, *Journal of Atmospheric*
798 *Chemistry*, 28, 195-207, 10.1023/a:1005877419395, 1997.

799 Grosjean, D.: Ambient Levels of Formaldehyde, Acetaldehyde, and Formic acid in
800 Southern Californic- Results of a One-year Base-line Study, *Environmental Science &*
801 *Technology*, 25, 710-715, 10.1021/es00016a016, 1991.

802 Hansen, D. A., Edgerton, E. S., Hartsell, B. E., Jansen, J. J., Kandasamy, N., Hidy, G. M.,
803 and Blanchard, C. L.: The southeastern aerosol research and characterization study: Part 1-
804 overview, *Journal of the Air & Waste Management Association*, 53, 1460-1471, 2003.

805 Hartmann, W. R., Santana, M., Hermoso, M., Andreae, M. O., and Sanhueza, E.: Diurnal
806 Cycles of Formic and Acetic Acids in the Northern Part of the Guayana Sheld, Venezuela,
807 *Journal of Atmospheric Chemistry*, 13, 63-72, 10.1007/bf00048100, 1991.

808 Hennigan, C. J., Bergin, M. H., Russell, A. G., Nenes, A., and Weber, R. J.: Gas/particle
809 partitioning of water-soluble organic aerosol in Atlanta, *Atmos. Chem. Phys.*, 9, 3613-
810 3628, 10.5194/acp-9-3613-2009, 2009.

811 Huey, L. G., Hanson, D. R., and Howard, C. J.: Reactions of SF₆- and I- with Atmospheric
812 Trace Gases, *Journal of Physical Chemistry*, 99, 5001-5008, 10.1021/j100014a021, 1995.

813 Huey, L. G., Tanner, D. J., Slusher, D. L., Dibb, J. E., Arimoto, R., Chen, G., Davis, D.,
814 Buhr, M. P., Nowak, J. B., Mauldin, R. L., Eisele, F. L., and Kosciuch, E.: CIMS
815 measurements of HNO₃ and SO₂ at the South Pole during ISCAT 2000, *Atmospheric*
816 *Environment*, 38, 5411-5421, 10.1016/j.atmosenv.2004.04.037, 2004.

817 Kawamura, K., Ng, L. L., and Kaplan, I. R.: Determination of Organic Acids (C₁-C₁₀) in
818 the Atmosphere, Motor Exhausts, and Engine Oils, *Environmental Science & Technology*,
819 19, 1082-1086, 10.1021/es00141a010, 1985.

820 Keene, W. C., Galloway, J. N., and Holden, J. D.: Measurement of Weak Organic Acidity
821 in Precipitation from Remote Areas of the World, *Journal of Geophysical Research-Oceans*
822 and Atmospheres, 88, 5122-5130, 10.1029/JC088iC09p05122, 1983.

823 Keene, W. C., and Galloway, J. N.: Organic Acidity in Precipitation of North America,
824 *Atmospheric Environment*, 18, 2491-2497, 10.1016/0004-6981(84)90020-9, 1984.

825 Kesselmeier, J., Bode, K., Hofmann, U., Muller, H., Schafer, L., Wolf, A., Ciccioli, P.,
826 Brancaleoni, E., Cecinato, A., Frattoni, M., Foster, P., Ferrari, C., Jacob, V., Fugit, J. L.,
827 Dutaur, L., Simon, V., and Torres, L.: Emission of short chained organic acids, aldehydes
828 and monoterpenes from *Quercus ilex* L. and *Pinus pinea* L. in relation to physiological
829 activities, carbon budget and emission algorithms, *Atmospheric Environment*, 31, 119-133,
830 10.1016/s1352-2310(97)00079-4, 1997.

831 Kesselmeier, J.: Exchange of short-chain oxygenated volatile organic compounds (VOCs)
832 between plants and the atmosphere: A compilation of field and laboratory studies, *Journal*
833 *of Atmospheric Chemistry*, 39, 219-233, 10.1023/a:1010632302076, 2001.

834 Khare, P., Kumar, N., Kumari, K. M., and Srivastava, S. S.: Atmospheric formic and acetic
835 acids: An overview, *Reviews of Geophysics*, 37, 227-248, 10.1029/1998rg900005, 1999.

836 Kim, S., Huey, L. G., Stickel, R. E., Tanner, D. J., Crawford, J. H., Olson, J. R., Chen, G.,
837 Brune, W. H., Ren, X., Leshner, R., Wooldridge, P. J., Bertram, T. H., Perring, A., Cohen,
838 R. C., Lefer, B. L., Shetter, R. E., Avery, M., Diskin, G., and Sokolik, I.: Measurement of
839 HO₂NO₂ in the free troposphere during the intercontinental chemical transport experiment
840 - North America 2004, *Journal of Geophysical Research-Atmospheres*, 112,
841 10.1029/2006jd007676, 2007.

842 Kuhn, U., Rottenberger, S., Biesenthal, T., Ammann, C., Wolf, A., Schebeske, G., Oliva,
843 S. T., Tavares, T. M., and Kesselmeier, J.: Exchange of short-chain monocarboxylic acids
844 by vegetation at a remote tropical forest site in Amazonia, *Journal of Geophysical*
845 *Research-Atmospheres*, 107, 18, 10.1029/2000jd000303, 2002.

846 Lee, B. H., Lopez-Hilfiker, F. D., Mohr, C., Kurten, T., Worsnop, D. R., and Thornton, J.
847 A.: An Iodide-Adduct High-Resolution Time-of-Flight Chemical-Ionization Mass
848 Spectrometer: Application to Atmospheric Inorganic and Organic Compounds,
849 *Environmental Science & Technology*, 48, 6309-6317, 10.1021/es500362a, 2014.

850 Lee, B. H., Lopez-Hilfiker, F. D., Veres, P. R., McDuffie, E. E., Fibiger, D. L., Sparks, T.
851 L., Ebben, C. J., Green, J. R., Schroder, J. C., Campuzano-Jost, P., Iyer, S., D'Ambro, E.
852 L., Schobesberger, S., Brown, S. S., Wooldridge, P. J., Cohen, R. C., Fiddler, M. N.,
853 Bililign, S., Jimenez, J. L., Kurtén, T., Weinheimer, A. J., Jaegle, L., and Thornton, J. A.:
854 Flight Deployment of a High-Resolution Time-of-Flight Chemical Ionization Mass
855 Spectrometer: Observations of Reactive Halogen and Nitrogen Oxide Species, *Journal of*
856 *Geophysical Research: Atmospheres*, 0, doi:10.1029/2017JD028082, 2018.

857 Liao, J., Sihler, H., Huey, L. G., Neuman, J. A., Tanner, D. J., Friess, U., Platt, U., Flocke,
858 F. M., Orlando, J. J., Shepson, P. B., Beine, H. J., Weinheimer, A. J., Sjostedt, S. J., Nowak,
859 J. B., Knapp, D. J., Staebler, R. M., Zheng, W., Sander, R., Hall, S. R., and Ullmann, K.:
860 A comparison of Arctic BrO measurements by chemical ionization mass spectrometry and
861 long path-differential optical absorption spectroscopy, *Journal of Geophysical Research-*
862 *Atmospheres*, 116, 10.1029/2010jd014788, 2011.

863 Lide, D. R.: *CRC handbook of chemistry and physics: a ready-reference book of chemical*
864 *and physical data*, CRC Press, Boca Raton, FL, 1995.

865 Lim, H. J., Carlton, A. G., and Turpin, B. J.: Isoprene forms secondary organic aerosol
866 through cloud processing: Model simulations, *Environmental Science & Technology*, 39,
867 4441-4446, 10.1021/es048039h, 2005.

868 Millet, D. B., Baasandorj, M., Farmer, D. K., Thornton, J. A., Baumann, K., Brophy, P.,
869 Chaliyakunnel, S., de Gouw, J. A., Graus, M., Hu, L., Koss, A., Lee, B. H., Lopez-Hilfiker,
870 F. D., Neuman, J. A., Paulot, F., Peischl, J., Pollack, I. B., Ryerson, T. B., Warneke, C.,
871 Williams, B. J., and Xu, J.: A large and ubiquitous source of atmospheric formic acid,
872 *Atmos. Chem. Phys.*, 15, 6283-6304, 10.5194/acp-15-6283-2015, 2015.

873 Molina, M. J., Ivanov, A. V., Trakhtenberg, S., and Molina, L. T.: Atmospheric evolution
874 of organic aerosol, *Geophys. Res. Lett.*, 31, 10.1029/2004gl020910, 2004.

875 Nah, T., Guo, H., Sullivan, A. P., Chen, Y., Tanner, D. J., Nenes, A., Russell, A., Ng, N.
876 L., Huey, L. G., and Weber, R. J.: Characterization of Aerosol Composition, Aerosol
877 Acidity and Organic Acid Partitioning at an Agriculture-intensive Rural Southeastern U.S.
878 Site, *Atmos. Chem. Phys. Discuss.*, in review, 10.5194/acp-2018-373, 2018.

879 Neuman, J. A., Ryerson, T. B., Huey, L. G., Jakoubek, R., Nowak, J. B., Simons, C., and
880 Fehsenfeld, F. C.: Calibration and evaluation of nitric acid and ammonia permeation tubes
881 by UV optical absorption, *Environmental Science & Technology*, 37, 2975-2981,
882 10.1021/es0264221, 2003.

883 Nguyen, T. B., Crouse, J. D., Teng, A. P., Clair, J. M. S., Paulot, F., Wolfe, G. M., and
884 Wennberg, P. O.: Rapid deposition of oxidized biogenic compounds to a temperate forest,
885 *Proc. Natl. Acad. Sci. U. S. A.*, 112, E392-E401, 10.1073/pnas.1418702112, 2015.

886 Nolte, C. G., Solomon, P. A., Fall, T., Salmon, L. G., and Cass, G. R.: Seasonal and spatial
887 characteristics of formic and acetic acids concentrations in the southern California
888 atmosphere, *Environmental Science & Technology*, 31, 2547-2553, 10.1021/es960954i,
889 1997.

890 Nowak, J. B., Huey, L. G., Russell, A. G., Tian, D., Neuman, J. A., Orsini, D., Sjostedt, S.
891 J., Sullivan, A. P., Tanner, D. J., Weber, R. J., Nenes, A., Edgerton, E., and Fehsenfeld, F.
892 C.: Analysis of urban gas phase ammonia measurements from the 2002 Atlanta Aerosol
893 Nucleation and Real-Time Characterization Experiment (ANARChE), *Journal of*
894 *Geophysical Research-Atmospheres*, 111, 14, 10.1029/2006jd007113, 2006.

895 Orzechowska, G. E., and Paulson, S. E.: Photochemical sources of organic acids. 1.
896 Reaction of ozone with isoprene, propene, and 2-butenes under dry and humid conditions
897 using SPME, *J. Phys. Chem. A*, 109, 5358-5365, 10.1021/jp050166s, 2005.

898 Pan, X., Underwood, J. S., Xing, J. H., Mang, S. A., and Nizkorodov, S. A.:
899 Photodegradation of secondary organic aerosol generated from limonene oxidation by

900 ozone studied with chemical ionization mass spectrometry, *Atmos. Chem. Phys.*, 9, 3851-
901 3865, 10.5194/acp-9-3851-2009, 2009.

902 Park, J., Gomez, A. L., Walser, M. L., Lin, A., and Nizkorodov, S. A.: Ozonolysis and
903 photolysis of alkene-terminated self-assembled monolayers on quartz nanoparticles:
904 implications for photochemical aging of organic aerosol particles, *Physical Chemistry*
905 *Chemical Physics*, 8, 2506-2512, 10.1039/b602704k, 2006.

906 Paulot, F., Wunch, D., Crounse, J. D., Toon, G. C., Millet, D. B., DeCarlo, P. F.,
907 Vigouroux, C., Deutscher, N. M., Abad, G. G., Notholt, J., Warneke, T., Hannigan, J. W.,
908 Warneke, C., de Gouw, J. A., Dunlea, E. J., De Maziere, M., Griffith, D. W. T., Bernath,
909 P., Jimenez, J. L., and Wennberg, P. O.: Importance of secondary sources in the
910 atmospheric budgets of formic and acetic acids, *Atmos. Chem. Phys.*, 11, 1989-2013,
911 10.5194/acp-11-1989-2011, 2011.

912 Seco, R., Penuelas, J., and Filella, I.: Short-chain oxygenated VOCs: Emission and uptake
913 by plants and atmospheric sources, sinks, and concentrations, *Atmospheric Environment*,
914 41, 2477-2499, 10.1016/j.atmosenv.2006.11.029, 2007.

915 Sindelarova, K., Granier, C., Bouarar, I., Guenther, A., Tilmes, S., Stavrakou, T., Muller,
916 J. F., Kuhn, U., Stefani, P., and Knorr, W.: Global data set of biogenic VOC emissions
917 calculated by the MEGAN model over the last 30 years, *Atmos. Chem. Phys.*, 14, 9317-
918 9341, 10.5194/acp-14-9317-2014, 2014.

919 Singh, H., Chen, Y., Tabazadeh, A., Fukui, Y., Bey, I., Yantosca, R., Jacob, D., Arnold,
920 F., Wohlfrom, K., Atlas, E., Flocke, F., Blake, D., Blake, N., Heikes, B., Snow, J., Talbot,
921 R., Gregory, G., Sachse, G., Vay, S., and Kondo, Y.: Distribution and fate of selected
922 oxygenated organic species in the troposphere and lower stratosphere over the Atlantic,
923 *Journal of Geophysical Research-Atmospheres*, 105, 3795-3805, 10.1029/1999jd900779,
924 2000.

925 Slusher, D. L., Pitteri, S. J., Haman, B. J., Tanner, D. J., and Huey, L. G.: A chemical
926 ionization technique for measurement of pernitric acid in the upper troposphere and the
927 polar boundary layer, *Geophys. Res. Lett.*, 28, 3875-3878, 10.1029/2001gl013443, 2001.

928 Slusher, D. L., Huey, L. G., Tanner, D. J., Chen, G., Davis, D. D., Buhr, M., Nowak, J. B.,
929 Eisele, F. L., Kosciuch, E., Mauldin, R. L., Lefer, B. L., Shetter, R. E., and Dibb, J. E.:
930 Measurements of pernitric acid at the South Pole during ISCAT 2000, *Geophys. Res. Lett.*,
931 29, 10.1029/2002gl015703, 2002.

932 Sorooshian, A., Ng, N. L., Chan, A. W. H., Feingold, G., Flagan, R. C., and Seinfeld, J.
933 H.: Particulate organic acids and overall water-soluble aerosol composition measurements
934 from the 2006 Gulf of Mexico Atmospheric Composition and Climate Study (GoMACCS),
935 *Journal of Geophysical Research-Atmospheres*, 112, 16, 10.1029/2007jd008537, 2007.

936 Sorooshian, A., Murphy, S. M., Hersey, S., Bahreini, R., Jonsson, H., Flagan, R. C., and
937 Seinfeld, J. H.: Constraining the contribution of organic acids and AMS m/z 44 to the
938 organic aerosol budget: On the importance of meteorology, aerosol hygroscopicity, and
939 region, *Geophys. Res. Lett.*, 37, 5, 10.1029/2010gl044951, 2010.

940 Souza, S. R., and Carvalho, L. R. F.: Seasonality influence in the distribution of formic and
941 acetic acids in the urban atmosphere of Sao Paulo City, Brazil, *Journal of the Brazilian*
942 *Chemical Society*, 12, 755-762, 2001.

943 Spaulding, R. S., Talbot, R. W., and Charles, M. J.: Optimization of a mist chamber (cofer
944 scrubber) for sampling water-soluble organics in air, *Environmental Science &*
945 *Technology*, 36, 1798-1808, 10.1021/es011189x, 2002.

946 Talbot, R. W., Beecher, K. M., Harriss, R. C., and Cofer, W. R.: Atmospheric
947 Geochemistry of Formic and Acetic Acids at a Mid-latitude Temperate Site, *Journal of*
948 *Geophysical Research-Atmospheres*, 93, 1638-1652, 10.1029/JD093iD02p01638, 1988.

949 Talbot, R. W., Mosher, B. W., Heikes, B. G., Jacob, D. J., Munger, J. W., Daube, B. C.,
950 Keene, W. C., Maben, J. R., and Artz, R. S.: Carboxylic Acids in the Rural Continental
951 Atmosphere over the Eastern United States during the Shenandoah Cloud and
952 Photochemistry Experiment, *Journal of Geophysical Research-Atmospheres*, 100, 9335-
953 9343, 10.1029/95jd00507, 1995.

954 Talbot, R. W., Dibb, J. E., Scheuer, E. M., Blake, D. R., Blake, N. J., Gregory, G. L.,
955 Sachse, G. W., Bradshaw, J. D., Sandholm, S. T., and Singh, H. B.: Influence of biomass
956 combustion emissions on the distribution of acidic trace gases over the southern Pacific
957 basin during austral springtime, *Journal of Geophysical Research-Atmospheres*, 104, 5623-
958 5634, 10.1029/98jd00879, 1999.

959 Veres, P., Roberts, J. M., Warneke, C., Welsh-Bon, D., Zahniser, M., Herndon, S., Fall, R.,
960 and de Gouw, J.: Development of negative-ion proton-transfer chemical-ionization mass
961 spectrometry (NI-PT-CIMS) for the measurement of gas-phase organic acids in the
962 atmosphere, *Int. J. Mass Spectrom.*, 274, 48-55, 10.1016/j.ijms.2008.04.032, 2008.

963 Veres, P., Roberts, J. M., Burling, I. R., Warneke, C., de Gouw, J., and Yokelson, R. J.:
964 Measurements of gas-phase inorganic and organic acids from biomass fires by negative-
965 ion proton-transfer chemical-ionization mass spectrometry, *Journal of Geophysical*
966 *Research-Atmospheres*, 115, 10.1029/2010jd014033, 2010.

967 Veres, P. R., Roberts, J. M., Cochran, A. K., Gilman, J. B., Kuster, W. C., Holloway, J. S.,
968 Graus, M., Flynn, J., Lefter, B., Warneke, C., and de Gouw, J.: Evidence of rapid production
969 of organic acids in an urban air mass, *Geophys. Res. Lett.*, 38, 10.1029/2011gl048420,
970 2011.

971 Vlasenko, A., George, I. J., and Abbatt, J. P. D.: Formation of volatile organic compounds
972 in the heterogeneous oxidation of condensed-phase organic films by gas-phase OH, *J. Phys.*
973 *Chem. A*, 112, 1552-1560, 10.1021/jp0772979, 2008.

974 Walser, M. L., Park, J., Gomez, A. L., Russell, A. R., and Nizkorodov, S. A.:
975 Photochemical aging of secondary organic aerosol particles generated from the oxidation
976 of d-limonene, *J. Phys. Chem. A*, 111, 1907-1913, 10.1021/jp0662931, 2007.

977 Xu, L., Guo, H. Y., Weber, R. J., and Ng, N. L.: Chemical Characterization of Water-
978 Soluble Organic Aerosol in Contrasting Rural and Urban Environments in the Southeastern
979 United States, *Environmental Science & Technology*, 51, 78-88, 10.1021/acs.est.6b05002,
980 2017.

981 YataVELLI, R. L. N., Mohr, C., Stark, H., Day, D. A., Thompson, S. L., Lopez-Hilfiker, F.
982 D., Campuzano-Jost, P., Palm, B. B., Vogel, A. L., Hoffmann, T., Heikkinen, L., Aijala,
983 M., Ng, N. L., Kimmel, J. R., Canagaratna, M. R., Ehn, M., Junninen, H., Cubison, M. J.,
984 Petaja, T., Kulmala, M., Jayne, J. T., Worsnop, D. R., and Jimenez, J. L.: Estimating the
985 contribution of organic acids to northern hemispheric continental organic aerosol,
986 *Geophys. Res. Lett.*, 42, 6084-6090, 10.1002/2015gl064650, 2015.

987 Zhang, R. Y., Suh, I., Zhao, J., Zhang, D., Fortner, E. C., Tie, X. X., Molina, L. T., and
988 Molina, M. J.: Atmospheric new particle formation enhanced by organic acids, *Science*,
989 304, 1487-1490, 10.1126/science.1095139, 2004.

990

991

992

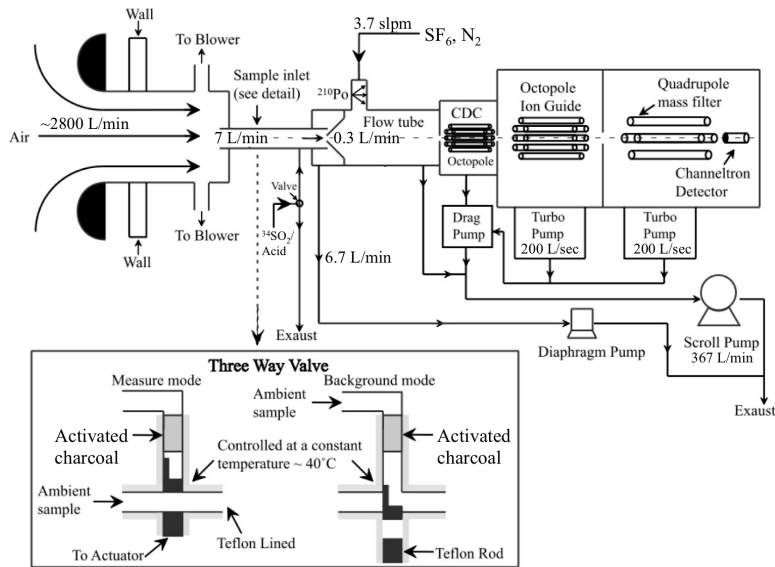
993

994

995

996

997



998

999 **Figure 1:** The CIMS instrument and inlet configuration used in the field study. The
 1000 automated three-way sampling valve is shown in the inset. The figure was adapted from
 1001 Liao et al. (2011).

1002

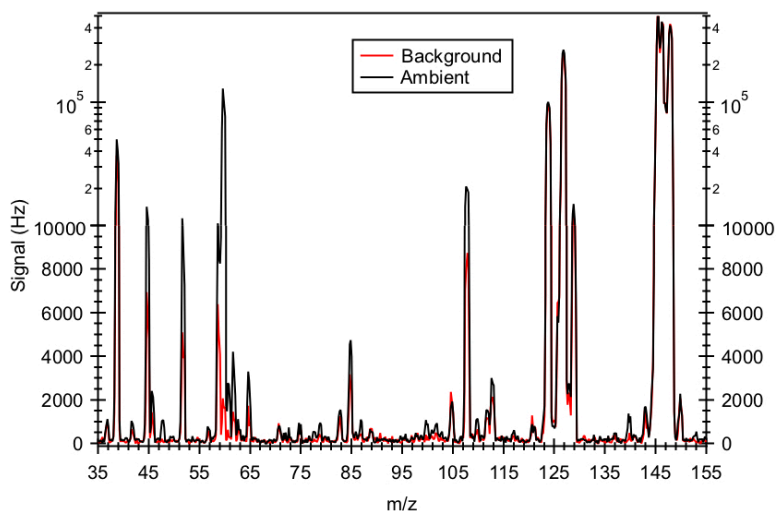
1003

1004

1005

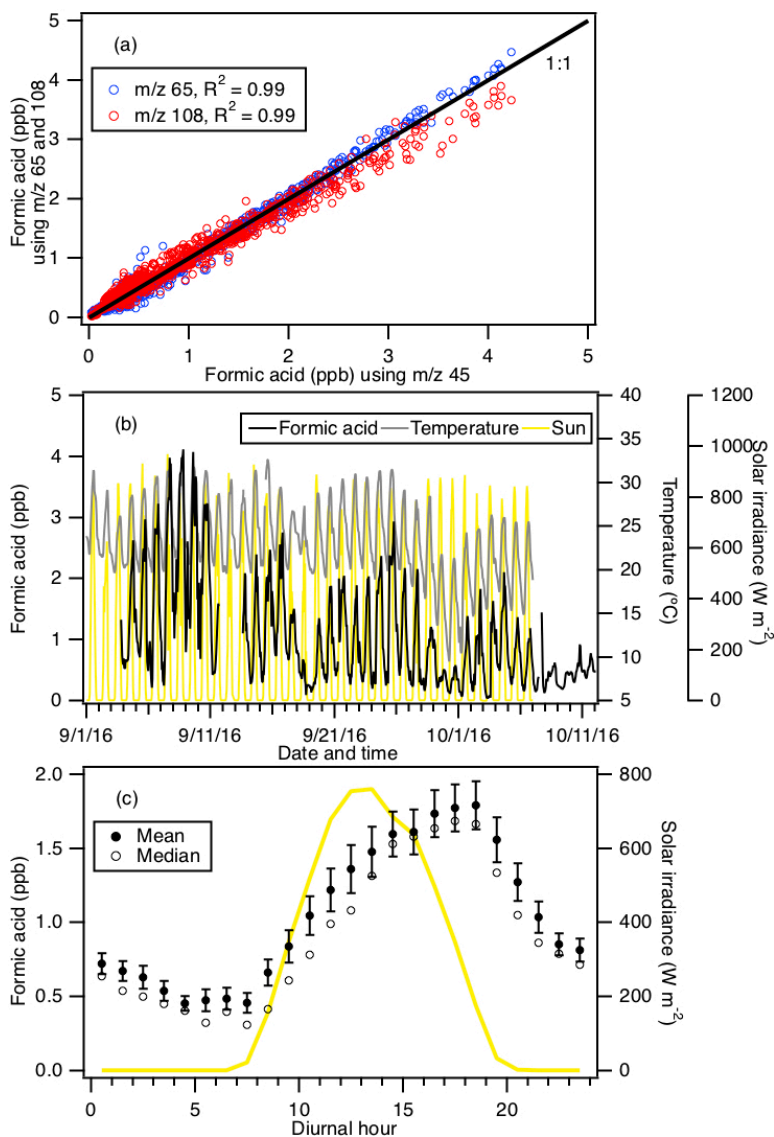
1006

1007



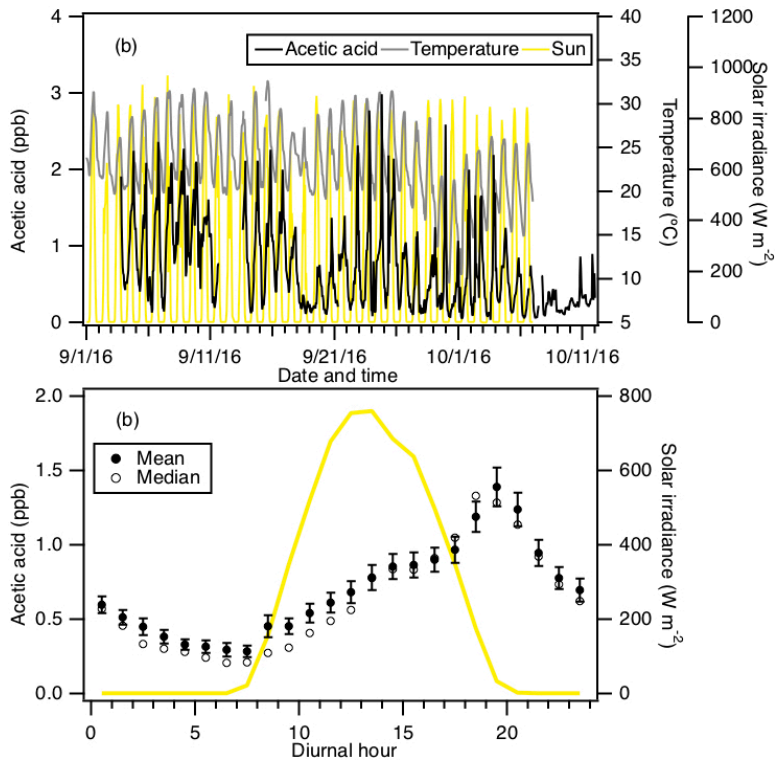
1008

1009 **Figure 2:** Mass spectrum of ambient air and background measured in Yorkville, Georgia
 1010 on 8 Sept 2016 using SF₆⁻. Note that the ³²SF₆⁻ reagent ion signal (at m/z 146) is saturated,
 1011 causing the sharp drop in its signal. As a result, the ion signal of its isotope ³⁴SF₆⁻ (at m/z
 1012 150) was monitored to determine if the reaction of SF₆⁻ with ambient water vapor and O₃
 1013 depleted SF₆⁻ reagent ions.



1014

1015 **Figure 3:** (a) Scatter plot comparison of ambient formic acid concentrations determined
 1016 using mass peaks m/z 45, 65 and 108. The three datasets correlated well with one another
 1017 ($R^2 = 0.99$). Linear regression of the data gave slopes of 1 (for m/z 65) and 0.95 (for m/z
 1018 108), indicating that all three mass peaks can be used to determine the formic acid
 1019 concentration. (b) Time series of formic acid concentration, temperature and solar
 1020 irradiance. All the data are displayed as 1-hour averages. (c) Diurnal profiles of formic acid
 1021 concentration (symbols) and solar irradiance (yellow line). All the concentrations represent
 1022 averages in 1-hour intervals and the standard errors are plotted as error bars.



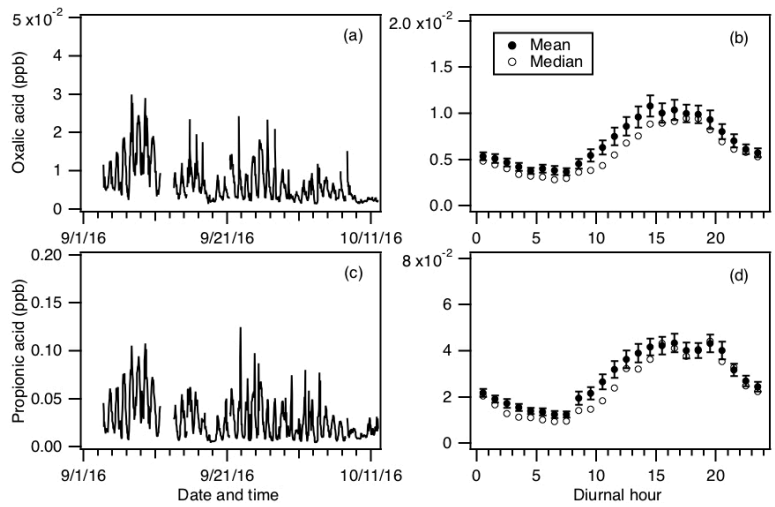
1023

1024 **Figure 4:** (a) Time series of acetic acid concentration, temperature and solar irradiance.
 1025 All the data are displayed as 1-hour averages. (c) Diurnal profiles of acetic acid (symbols)
 1026 and solar irradiance (yellow line). All the concentrations represent averages in 1-hour
 1027 intervals and the standard errors are plotted as error bars.

1028

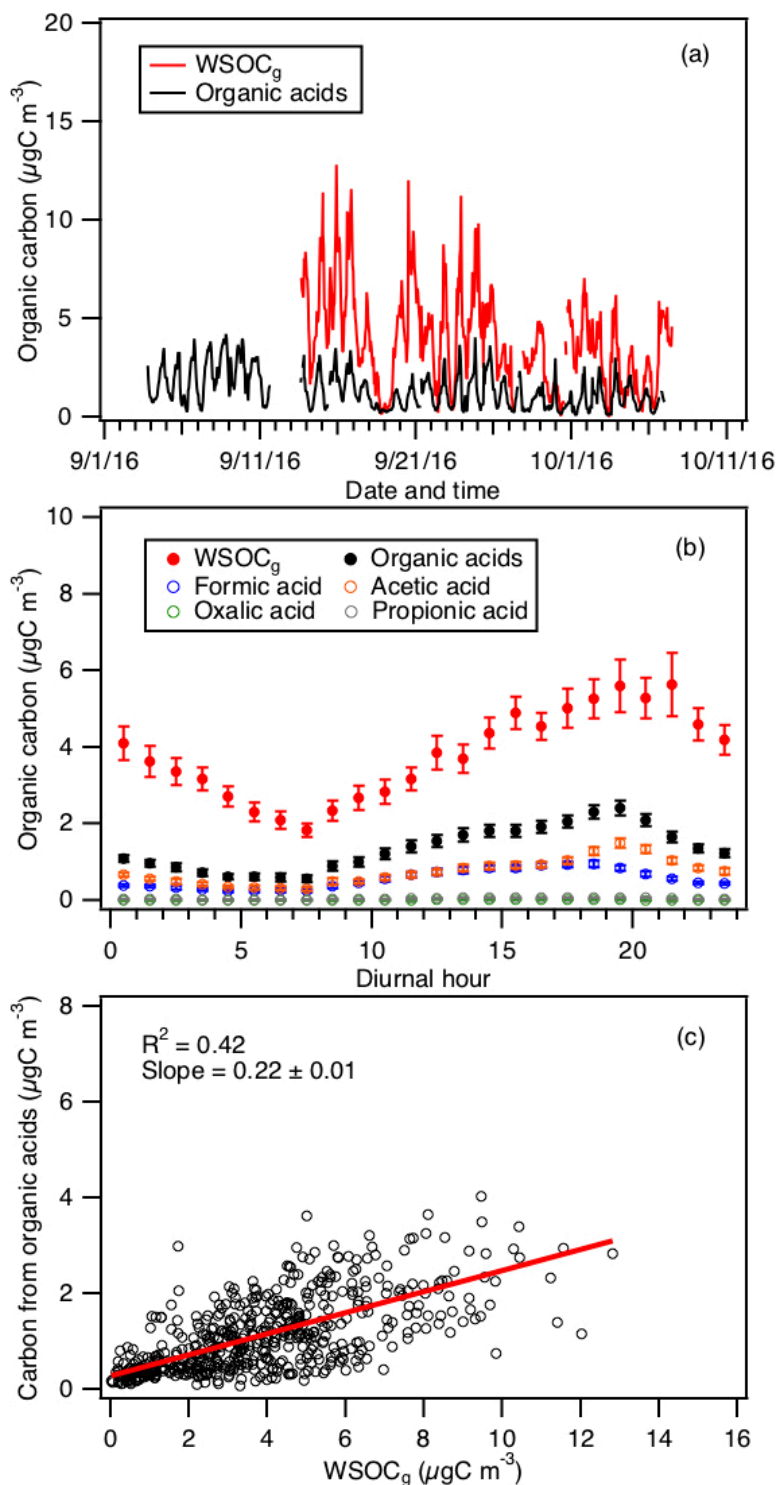
1029

1030



1031

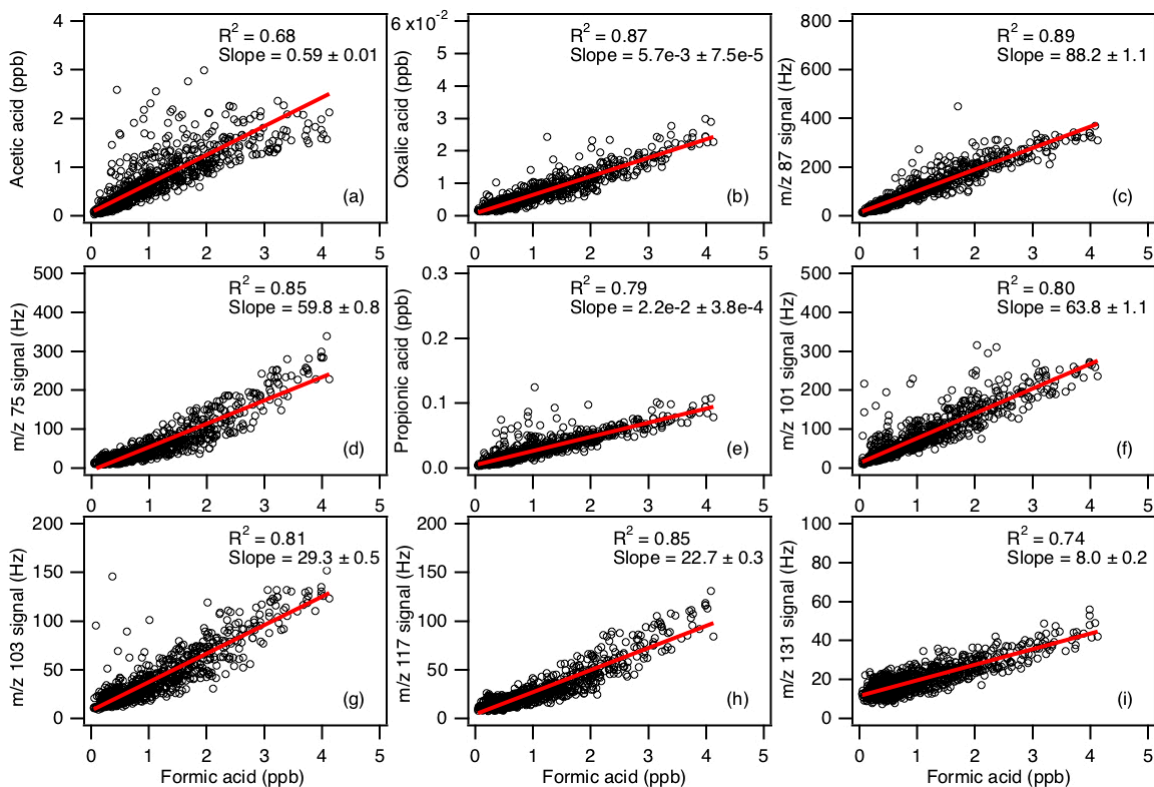
1032 **Figure 5:** Time series of concentrations of (a) oxalic and (c) propionic acids measured
 1033 during the field study. All the data are displayed as 1-hour averages. Their corresponding
 1034 diurnal profiles are shown in (b) and (d), respectively. The diurnal profile concentrations
 1035 represent averages in 1-hour intervals and the standard errors are plotted as error bars.



1036

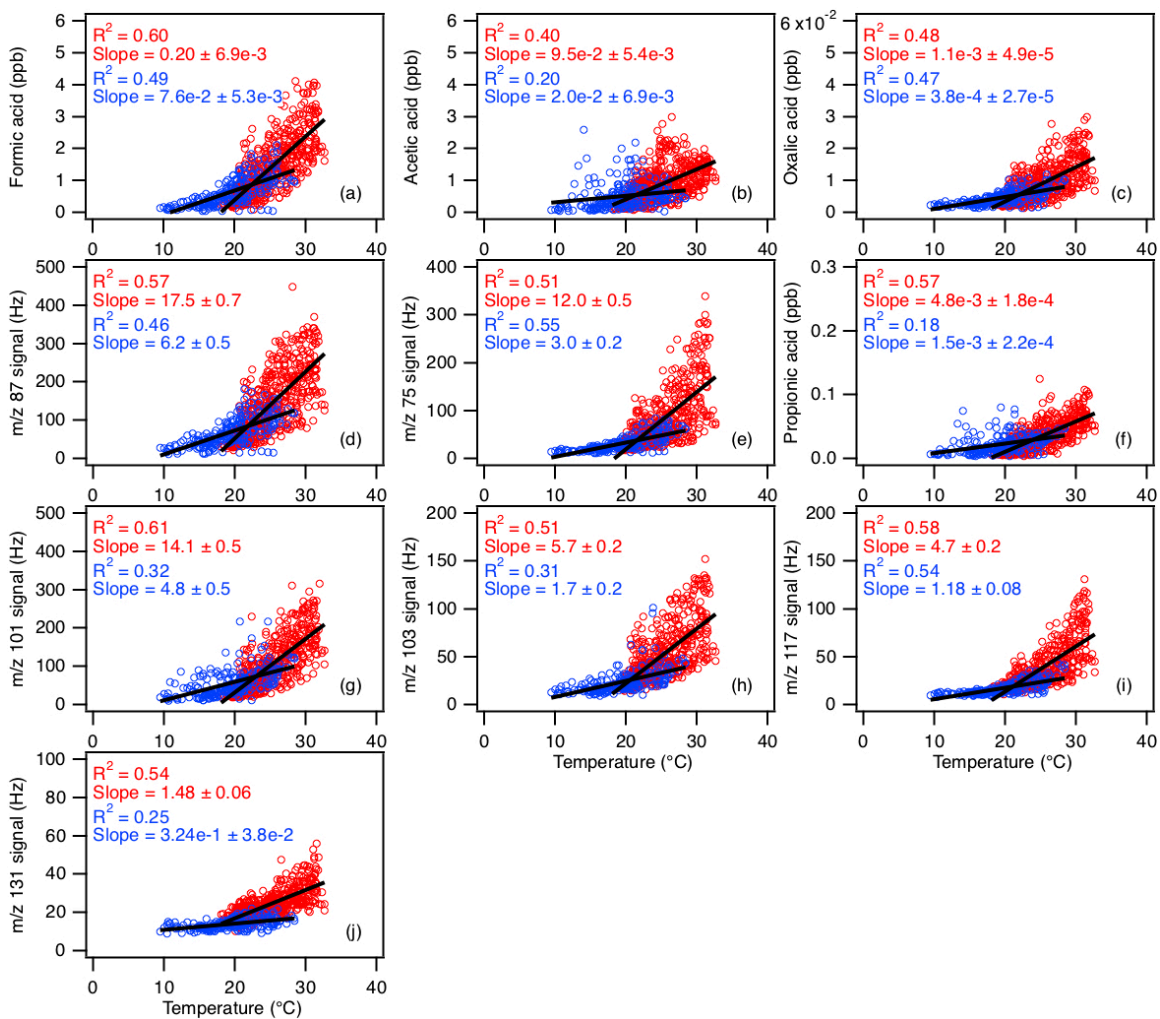
1037 **Figure 6:** (a) Time series of WSOC_g and the total organic carbon contributed by formic,
 1038 acetic, oxalic and propionic acids. All the data are displayed as 1-hour averages. (b) Diurnal
 1039 profiles of WSOC_g and the total organic carbon contributed by formic, acetic, oxalic and
 1040 propionic acids. Also shown are the diurnal profiles of the organic carbon contributed by

1041 the individual organic acids. All the concentrations represent the mean hourly averages and
1042 the standard errors are plotted as error bars. (c) Scatter plot of total organic carbon
1043 contributed by formic, acetic, oxalic and propionic acids with $WSOC_g$.



1044

1045 **Figure 7:** Scatter plots of concentrations (or ion signals) of the measured organic acids
1046 with formic acid concentration. All the data are displayed as 1-hour averages. Red lines
1047 shown are linear fits to the data.



1048

1049 **Figure 8:** Scatter plots of concentrations (or ion signals) of the measured organic acids
 1050 with ambient temperature. The red symbols are data collected from 3 to 27 Sept, while the
 1051 blue symbols are data collected from 28 Sept onwards. All the data are displayed as 1-hour
 1052 averages. Black lines shown are linear fits to the datasets.

1053

1054

1055

1056

1057

1058 **Table 1:** Summary of organic acids of interest, their detection limits and sensitivities of
 1059 their X⁻ and X⁻•HF ions^a

Organic Acid	Detection limit (ppt) ^b	Sensitivity (Hz ppt ⁻¹)	
		X ⁻	X ⁻ •HF
Formic acid	30	1.29 ± 0.22	0.29 ± 0.05
Acetic acid	60	1.46 ± 0.29	0.30 ± 0.06
Oxalic acid	1	6.38 ± 0.32	0.97 ± 0.05
Butyric acid	30	0.41 ± 0.01	0.12 ± 0.004
Glycolic acid	2	5.53 ± 0.11	1.64 ± 0.03
Propionic acid	6	2.05 ± 0.02	1.26 ± 0.01
Valeric acid	10	0.76 ± 0.008	0.35 ± 0.004

1060 ^aOnly organic acids with calibration measurements are shown.

1061 ^bDetection limits are approximated from 3 times the standard deviation values (3σ) of the
 1062 ion signals measured during background mode. Shown here are the average detection limits
 1063 of the organic acids for 2.5 min averaging periods which corresponds to the length of a
 1064 background measurement at a 4 % duty cycle for each mass.